UCLA
COMPUTATIONAL AND APPLIED MATHEMATICS

Resistive Instabilities in Rapidly Rotating Fluids: Linear Theory of the g-Mode

Weijia Kuang
Paul H. Roberts

December 1990

CAM Report 90-28

Department of Mathematics
University of California, Los Angeles
Los Angeles, CA. 90024-1555

RESISTIVE INSTABILITIES IN RAPIDLY ROTATING FLUIDS: LINEAR THEORY OF THE g-MODE[1]

WEIJIA KUANG
Department of Mathematics, University of California, Los Angeles, California, CA 90024
PAUL H. ROBERTS
Center for Earth and Planetary Interiors, Institute of Geophysics and Planetary Physics, University of California, Los Angeles, California, CA 90024[2]

Received:

The linear stability is examined of a stratified sheet pinch in a rapidly rotating fluid lying hydrostatically in a gravitational field, $\mathbf{g}$, perpendicular to the sheet. The sheet pinch is a horizontal layer of inviscid, Boussinesq fluid of electrical conductivity σ, magnetic permeability μ, and almost uniform density ρ_0, confined between two perfectly conducting planes $z = 0, d$, where z is height. The prevailing magnetic field, $\mathbf{B}_0(z)$, is horizontal; it is unidirectional at each z level, but that direction depends on z. The layer rotates about the vertical with a large angular velocity, $\mathbf{\Omega}$: $\Omega \gg V_A/d$, where $V_A = B_0/\sqrt{(\mu\rho_0)}$ is the Alfvén velocity and μ is the magnetic permeability. The Elsasser number, $\Lambda = \sigma B_0^2/2\Omega\rho_0$, measures σ. A (modified) Rayleigh number, $R = g\beta d^2/\rho_0 V_A^2$, measures the buoyancy force, where $\boldsymbol{\beta}$ is the imposed density gradient, antiparallel to gravity.

The gravitationless case, $R = 0$, was studied in Part 1 of this series. It was shown that "resistive instabilities", known as "tearing modes", exist when Λ is large enough, the horizontal wavenumber, k, of the instability is small enough, and when at least one "critical level" exists within the layer, this a value of z at which $\mathbf{B}$ is perpendicular to the horizontal wavevector, $\mathbf{k}$. When R is sufficiently large, instability occurs for any $\mathbf{k}$; critical layers need not exist; k need not be small. For each $\mathbf{k}$, a critical value, $R_c(\mathbf{k})$, exists such that if $R > R_c$ the layer is ideally unstable (i.e. unstable for $\Lambda = \infty$); when a critical level exists, R_c is independent of k. When $\Lambda \neq \infty$, the growth rate, s, of instability becomes that of the ideal mode as $\Lambda \to \infty$, but for $R < R_c$ resistive instabilities arise, i.e. those in which $s \to +0$ as $\Lambda \to \infty$. These "g-modes" are the main topic of this study. When critical levels are absent, they grow no more rapidly (except near $R = R_c$) than the rate at which $\mathbf{B}$ itself evolves ohmically; when a critical level exists, and especially when k is large (the so-called "fast g-modes", also studied here), they grow more rapidly. When $\Lambda \gg 1$ and one or more critical levels exist, s is determined *entirely* by the structure of the "critical layer" surrounding a critical level.

When $R > 0$, instability is always "direct" ($\Im s = 0$), but when $R < 0$, overstability may occur ($\Im s \neq 0$, $\Re s > 0$). Since such a mode bifurcates from a tearing instability, it exists only if Λ is enough, k is small enough, and a critical level exists.

The principal example studied here is force-free ($\mathbf{J}_0 \times \mathbf{B}_0 = 0$) since the chosen electric current density, $\mathbf{J}_0 = \nabla \times \mathbf{B}_0/\mu$, is a multiple of $\mathbf{B}_0$. Both are of constant strength, but turn uniformly in direction with height.

KEY WORDS: resistive instability, tearing mode, rotating magnetohydrodynamics.

---

[1] Contribution no.2 of the Center for Earth and Planetary Interiors, UCLA.

[2] Also at Department of Mathematics, University of California, Los Angeles, California, CA 90024.

1. INTRODUCTION

This is the second paper of a series devoted to resistive instabilities of sheared magnetic fields in rapidly rotating fluid systems of high electrical conductivity. As such, the series represents a generalization of the better-known magnetohydrodynamic ("MHD") studies of non-rotating systems (e.g. Furth *et al*, 1963), studies that have aimed at a better understanding of the nature of instabilities to which a magnetically confined laboratory plasma may be prone. Although these "classical" investigations are usually, because of the importance of Coriolis forces, not directly relevant to systems of cosmic scale, there are significant similarities. In this series, we reopen the study of instability mechanisms, with the crucial, "non-classical" difference that the Coriolis forces provide the dominant part of the inertial forces in the equation of fluid motion. There are two immediate consequences, one physical and one mathematical: physically, instability is postponed and, when it occurs, it takes longer to develop; mathematically, the differential system to be analysed is of higher differential order. The underlying energy sources for the instabilities are, of course, the same in both cases. This has already been seen in the study of the tearing mode to which the first paper in this series was devoted (Kuang and Roberts, 1990, hereafter referred to as "Part 1"); it will also emerge from the present study of the g-mode.

Although the model considered here is highly idealized, it is perhaps the canonical example of an instability that may well be relevant in geophysical and astrophysical contexts. It is highly desirable for the development of geodynamo theory to understand the nature and timescales of all MHD instabilities to which the highly rotating, stratified fluid core may be subject, and this paper forms a modest addition to the rapidly growing literature devoted to those questions. We refer the reader to recent reviews by Braginsky (1989) and Fearn (1989), in which references to earlier work are given.

"Tearing" is the present participle used to describe a purely magnetic instability that draws its energy from the reconnection of the field lines of an ambient magnetic field, $\mathbf{B}_0$, that is "sheared", i.e. turns in direction, e.g.

$$\mathbf{B}_0 = B_{0x}(z)\hat{\mathbf{x}} + B_{0y}(z)\hat{\mathbf{y}}\,, \tag{1.1}$$

where (x, y, z) are Cartesian coordinates and $\hat{\mathbf{x}}$ and $\hat{\mathbf{y}}$ are the unit vectors parallel to Ox and Oy. In Part 1 we supposed that the angular velocity, $\mathbf{\Omega}$, is in the z-direction, and we focussed attention on the simplest example of (1.1), namely a field of constant strength, B_0, which turns continuously in direction about the vertical: we supposed that

$$\mathbf{B}_0 = B_0[\hat{\mathbf{x}}\,\cos(qz/d) + \hat{\mathbf{y}}\,\sin(qz/d)]\,, \tag{1.2}$$

in a layer confined by two impermeable walls, $z = 0$ and $z = d$. For convenience, these walls were supposed to be perfect electrical conductors.

Relying as it does on field line reconnection, tearing can occur only in a fluid of finite electrical conductivity, σ, i.e. for finite Elsasser numbers,

$$\Lambda = \frac{\sigma B_0^2}{2\Omega\rho_0} = \frac{V_A^2}{2\Omega\eta}\,, \tag{1.3}$$

where ρ_0 is the fluid density, assumed constant. Here $V_A = B_0/\sqrt{(\mu_o\rho_0)}$ is the Alfvén velocity, $\eta = 1/\mu_0\sigma$ is the magnetic diffusivity and μ_0 is the permeability of free space

(S.I. units). As discussed in Part 1, the Elsasser number is the ratio, τ_η/τ_s, of the diffusive timescale $\tau_\eta = d^2/\eta$ and the dynamic timescale, which (in the case of the rapidly rotating systems studied here, in which $\Omega \gg V_A/d$) is the so-called "slow MHD timescale", $\tau_s = 2\Omega d^2/V_A^2$.

The g-mode studied here relies on gravitational energy release, through the presence of a uniform gravitational acceleration, $\mathbf{g} = -g\hat{\mathbf{z}}$ and a uniform adverse density gradient, β; in the undisturbed equilibrium state: $\nabla\rho_0 = \beta\hat{\mathbf{z}}$; ρ_0 is no longer constant, but varies so little that the Boussinesq approximation is justified. Buoyancy forces introduce a new timescale,

$$\tau_g = \left(\frac{\rho_0}{g\beta}\right)^{1/2}, \tag{1.4}$$

which, if the layer were bottom heavy, would be the reciprocal of the Brunt frequency. The strength of the buoyancy forces is measured by a dimensionless "Rayleigh number", which in this paper is taken to be the ratio, $(\tau_A/\tau_g)^2$ where $\tau_A = d/V_A$, so that

$$R = \frac{g\beta d^2}{\rho_0 V_A^2}. \tag{1.5}$$

The magnetic field constrains gravitational overturning, a constraint that is particularly stringent when the fluid is perfectly conducting ($\sigma = \Lambda = \infty$) and cannot by Alfvén's theorem detach itself from the lines of force on which it lies. The distortion of field involved in overturning the layer is massive, and can be accomplished only if gravitational energy is available to supply the necessary added magnetic energy. Consequently, the system can become unstable only if R exceeds a certain critical threshold value, R_c; see Section 3. A finitely conducting fluid is not strictly constrained by Alfvén's theorem, and can detach itself from field lines at a rate proportional to the resistivity and the field gradients. It can therefore overturn by drifting through the field lines, which are not required to overturn with it and need not be massively distorted. Thus, when $\Lambda \neq \infty$, instability occurs when R is less than R_c. Indeed when density diffusion is ignored, as it is in this paper, such "resistive instabilities" occur for all positive R. Since the instability depends on detaching fluid from field lines, it proceeds at a rate that (except for disturbances of small wavelength – see Section 4) vanishes in the limit $\Lambda \to \infty$.

As in the case of tearing, critical layers have a particular significance for g–mode instability. Critical levels occur at any and all heights, z, at which the wave vector, $\mathbf{k}$, of the perturbation is perpendicular to $\mathbf{B}_0$, and at which therefore the overturning motions "interchange" lines of force of $\mathbf{B}_0$ as a whole without bending them in a circulation that releases gravitational energy in the "critical layer" surrounding the critical level.

Mechanisms of this type will be studied in Section 4 below. Ideal and resistive instabilities arising when $\mathbf{k}\cdot\mathbf{B}_0$ is nowhere zero are of less interest, but are studied for completeness in Sections 3 and 4. In Section 5 we report on another instability to which field (1.2) is subject when Λ is large enough, an instability that arises for *negative* R, corresponding to a *bottom*-heavy equilibrium. Section 2 is devoted to the basic equations and boundary conditions. As in Part 1, only questions of linear stability are studied here.

2. Basic equations and boundary conditions

As in Part 1, we suppose that the rotation of the system is large, i.e. $\Omega \gg V_A/d$. We therefore adopt the magnetostrophic approximation, in which the equation of motion reduces to

$$2\rho_0 \mathbf{\Omega}\times\mathbf{V} = -\nabla P + \mathbf{J}\times\mathbf{B} + \rho_0 C\mathbf{g}\,, \tag{2.1}$$

where $\mathbf{V}$ is the fluid velocity, P is the reduced pressure (pressure divided by ρ_0 and including centrifugal forces), $\mathbf{J}$ $(= \mu^{-1}\nabla\times\mathbf{B})$ is the electric current density, and $C = \Delta\rho/\rho_0$ measures the density excess, $\Delta\rho$, of the stratification. The remaining equations are

$$\partial_t \mathbf{B} \;=\; \nabla\times(\mathbf{V}\times\mathbf{B}) \;+\; \eta\nabla^2\mathbf{B}\,, \tag{2.2}$$

$$(\partial_t \;+\; \mathbf{V}\cdot\nabla)C \;=\; 0\,, \tag{2.3}$$

$$\nabla\cdot\mathbf{V} = 0\,, \qquad \nabla\cdot\mathbf{B} = 0\,. \tag{2.4, 2.5}$$

(Here ∂_t stands for the Eulerian time derivative.)

It will be seen that diffusive processes are included only in the electromagnetic induction equation (2.2). There is no viscosity in (2.1), and there is no diffusion of density differences in (2.3), an equation that states that the mass contained in each fluid element is preserved in the isochoric motion assumed in the Boussinesq approximation (2.4).

The basic state whose stability is studied is one of rest in the prevailing field (1.1),

$$\mathbf{V}_0 \;=\; 0, \qquad \mathbf{B}_0 \;=\; B_{0x}\hat{\mathbf{x}} \;+\; B_{0y}\hat{\mathbf{y}}, \qquad C_0 \;=\; -\beta z/\rho_0, \qquad \ldots\,, \tag{2.6}$$

and its linear stability is decided from the equations obtained by writing

$$\mathbf{V} \;=\; \mathbf{V}_0 \;+\; \mathbf{v}, \qquad \mathbf{B} \;=\; \mathbf{B}_0 \;+\; \mathbf{b}, \qquad C \;=\; C \;+\; c, \qquad \ldots\,, \tag{2.7}$$

substituting into (2.1) – (2.5), and discarding all squares and products of the perturbed variables, $\mathbf{v}$, $\mathbf{b}$, c, ... The resulting linear system is solved subject to appropriate boundary conditions at $z = 0$ and $z = d$ (see below).

It transpires that the question of linear stability can be decided through a study of the normal modes in which $\mathbf{b}$ has the form

$$\mathbf{b} \;=\; \hat{\mathbf{b}}(z)\exp[i(k_x x \;+\; k_y y) \;+\; st]\,, \tag{2.8}$$

and similarly for $\mathbf{v}$, c, ... If $\Re s > 0$ for any such mode, the system is unstable; if $\Re s \leq 0$ for all modes, it is linearly stable. (The carat $\hat{}$ on $\hat{\mathbf{b}}$ and other perturbed quantities will henceforward be omitted.)

In (2.8) and what follows, we transform to dimensionless variables, as defined in Part 1. We then have

$$v_z = \frac{i}{F}\left\{\frac{1}{\Lambda}(D^2 - k^2) - s\right\} b_z\,, \tag{2.9}$$

$$j_z = \frac{\bar{F}}{F} b_z - \frac{1}{F} D\left[\frac{1}{F}\left\{\frac{1}{\Lambda}(D^2 - k^2) - s\right\}\right] b_z\,, \tag{2.10}$$

$$\begin{aligned}\omega_z = {} & \frac{i}{\Lambda F}\left\{2D\left(\frac{\bar{F}}{F}\right) Db_z + D^2\left(\frac{\bar{F}}{F}\right) b_z\right\} \\ & - \frac{i}{F}\left\{\frac{1}{\Lambda}(D^2 - k^2) - s\right\} \frac{1}{F} D\left[\frac{1}{F}\left\{\frac{1}{\Lambda}(D^2 - k^2) - s\right\} b_z\right]\,,\end{aligned} \tag{2.11}$$

$$D\omega_z - i[F(D^2 - k^2) - D^2 F]b_z + \frac{Rk^2}{s} v_z = 0\,, \tag{2.12}$$

where $\boldsymbol{\omega} = \nabla \times \mathbf{v}$ is the vorticity, $D = d/dz$, $k = \sqrt{(k_x^2 + k_y^2)}$, and

$$F = k_x B_{0x} + k_y B_{0y}, \qquad \bar{F} = k_x J_{0x} + k_y J_{0y} = D(k_y B_{0x} - k_x B_{0y})\,. \tag{2.13}$$

The system (2.9) – (2.12) differs from that solved in Part 1 only by the presence of the last term on the left-hand side of (2.12), but this difference is crucial. It accounts for the essentially dissimilar character of the g-modes, both physically and mathematically. One immediate distinction is apparent from (2.12): when $R \neq 0$, there can be no transition from instability to stability via a direct mode.

As in Part 1, the governing system is of sixth order, and to close the problem we shall apply the same three boundary conditions at each wall:

$$v_z = b_z = Dj_z = 0\,, \qquad \text{at} \qquad z = 0, 1\,. \tag{2.14}$$

By elimination we find that

$$\begin{aligned}& D\left[\left[\frac{1}{F}\left\{\frac{1}{\Lambda}(D^2 - k^2) - s\right\} \frac{1}{F} D\left[\frac{1}{F}\left\{\frac{1}{\Lambda}(D^2 - k^2) - s\right\} b_z\right]\right]\right] \\ & - \frac{1}{\Lambda} D\left[\frac{1}{F}\left\{2D\left(\frac{\bar{F}}{F}\right) Db_z + D^2\left(\frac{\bar{F}}{F}\right) b_z\right\}\right] + F(D^2 - k^2)b_z - (D^2 F)b_z \\ & - \frac{Rk^2}{sF}\left\{\frac{1}{\Lambda}(D^2 - k^2) - s\right\} b_z = 0\,,\end{aligned} \tag{2.15}$$

where

$$b_z = D^2 b_z = D^4 b_z - \Lambda F \bar{F} D b_z - \frac{3\Lambda D F}{F}\left\{\frac{1}{\Lambda}(D^2 - k^2) - s\right\} D b_z = 0, \quad \text{at} \quad z = 0, 1\,. \tag{2.16}$$

If we write

$$k_x = -k \sin\theta, \qquad k_y = k \cos\theta, \tag{2.17}$$

we have, for the field (1.2),

$$F = \bar{F}/q = k \sin q(z - z_c), \qquad \text{where} \qquad z_c = \theta/q, \tag{2.18}$$

and the first combination of terms on the right-hand side of (2.11) is absent, as are the $\bar{F}$ terms in (2.15). The $\bar{F}$ term remaining in (2.16) nevertheless destroys the symmetry or antisymmetry of the eigenfunctions even when F is symmetric about the mid-plane [$F(z) \equiv F(1 - z)$]. This is particularly evident when j_z is graphed; see below and also the discussion in Part 1.

In what follows, as in Part 1, much hinges on the behavior of the solutions in the "critical layers", regions that are narrow when Λ is large, and which surround the "critical levels" at which F vanishes. We may distinguish four possibilities:

(a) there are no critical levels; F has no zero in $0 < z < 1$;
(b) there is one critical level in $0 < z < 1$, namely $z = z_c$;
(c) there are two critical levels in $0 < z < 1$, namely $z = z_c$ and $z = z_c + \pi/q$, corresponding to θ and $\theta + \pi$ in (2.18), directions of k that are both orthogonal to $\mathbf{B}_0$. [Without loss of generality, we may take z_c to be the lower of these two levels.];
(d) there are three or more critical levels in $0 < z < 1$.

Tearing instabilities cannot occur in case (a), and also cannot arise in the other cases unless k is small enough. Attention was therefore focussed in Part 1 on cases (b) and (c); case (d) was excluded because it added complications without enlightenment. Of course, tearing instabilities are governed by the present theory when $R = 0$, and instabilities very similar to the tearing modes arise when R is sufficiently small. We aim to avoid going over the same ground as that covered in Part 1. We shall therefore mainly investigate situations in which the the magnetic field is not the main source of energy for the instabilities, as for example in case (a), or in case (b) at moderate or large k. We shall examine some resistive g-modes in case (c) but only briefly; we shall not look at case (d) at all.

3. Ideal modes

In this section we study the ideal fluid: $\Lambda = \infty$. To motivate (3.2) below, we first consider briefly the limit $\Lambda \to \infty$. The system (2.9) – (2.12) becomes of second order,

$$D\left[\left(F^2 + \frac{s_0^2}{F^2}\right) Dv_z\right] + k^2(R - F^2)v_z = 0, \tag{3.1}$$

and not all conditions (2.14) can be satisfied. Boundary layers can, however, be constructed that are vanishingly thin in the limit $\Lambda \to \infty$ and are passive, i.e. that affect neither the "outer solution" (3.1) nor the eigenvalue s_0 to leading order; it is necessary only that solutions to (3.1) obey

$$v_z(0) = v_z(1) = 0. \tag{3.2}$$

In this Section we shall suppose that (3.1) is satisfied *everywhere* in $0 < z < 1$, i.e. we shall suppose that $\Lambda = \infty$, rather than $\Lambda \to \infty$. In the latter case there is, in case (b), a diffusive critical layer surrounding the critical level $z = z_c$; in case (a), a diffusive layer appears at a boundary. In both cases, the structure of the solutions and the growth rates may be, as we shall see in Section 4, radically different from the one we consider here.

In case (a), (3.1) has no singularities in $0 < z < 1$, and the task of finding nontrivial solutions obeying (3.2) is a straightforward numerical operation. Indeed, the solution can be obtained analytically when $k \gg 1$, as is shown at the end of this Section. Table 1 shows s_0 as a function of R for one instance of case (a), namely $q = \frac{1}{2}\pi$, $k_x = k_y = 1$. It may be seen that inequality (3.7) is satisfied by the unstable modes.

In case (b), the solutions of (3.1) are regular even at the critical point and Dv_z/F^2 is bounded there. But (3.1) possesses regular singularities not only at $z = z_c$ but also at the four roots of

$$F^4 + s_0^2 = 0. \tag{3.3}$$

If s_0^2 is real and negative, two of these roots lie on the real axis, and the solutions of (3.1) are logarithmic in their neighborhood. It is then impossible to satisfy (3.2). This, stable discrete modes can exist, but only if their frequencies exceed $F^2_{\max}$. We shall consider the case $s_0^2 < 0$ no further here, but shall be particularly interested in the unstable modes for which (see below) $s_0 > 0$.

In case (a), it follows quickly from (3.1) and (3.2) that

$$\int_0^1 \left[\left(F^2 + \frac{s_0^2}{F^2} \right) |Dv_z|^2 + k^2(F^2 - R)|v_z|^2 \right] dz = 0. \tag{3.4}$$

This is also true in case (b) since Dv_z/F is regular at $z = z_c$. It follows in both cases that s_0^2 is real, and that a necessary condition for instability ($s_0^2 > 0$) is

$$R > F^2_{\min}. \tag{3.5}$$

The tearing modes ($R = 0$) are therefore not unstable. According to (2.18), a nonzero minimum of F^2 [case (a)] can occur for model (1.2) only at $z = 0$ or $z = 1$.

Suppose that $R > 0$ and that the system is unstable : $s_0^2 > 0$. For the growing mode, $s_0 > 0$, we have

$$\int_0^1 \left(F^2 + \frac{s_0^2}{F^2} \right) |Dv_z|^2 \, dz \geq 2s_0 \int_0^1 |Dv_z|^2 \, dz \geq 2\pi^2 s_0 \int_0^1 |v_z|^2 \, dz, \tag{3.6}$$

so that by (3.4)

$$[2\pi^2 s_0 + k^2(F^2_{\min} - R)] \int_0^1 |v_z|^2 \, dz \leq 0, \tag{3.7}$$

from which a bound on the growth rate follows:

$$s_0 \leq \frac{k^2}{2\pi^2}(R - F^2_{\min}). \tag{3.8}$$

The transition, $R \to R_c$, towards stability may be investigated by considering the limit $s_0^2 \to 0+$, in which (3.1) becomes

$$D(F^2 Dv_z) + k^2(R - F^2)v_z = 0. \tag{3.9}$$

In case (a), this equation is non-singular in $0 < z < 1$, and $R_c(k)$ is located by straightforward integration[3] linked to a search for nontrivial solutions that obey (3.2). For $q = \frac{1}{2}\pi$ and $k_x = k_y = 1$, we find that $R_c \approx 8.5904$; see also Table 1. Although the system is ideally stable for $R < R_c$, it is resistively unstable, as we shall see in the next Section.

In case (b) the limit $s_0^2 \to 0+$ requires asymptotic analysis. Equation (3.9) possesses a regular singularity at $z = z_c$, and it is easy to establish by the method of Frobenius that

$$v_z \sim \begin{cases} A_1^+(z - z_c)^{\alpha_1} + A_2^+(z - z_c)^{\alpha_2}, & z \to z_c+, \\ A_1^-(z_c - z)^{\alpha_1} + A_2^-(z_c - z)^{\alpha_2}, & z \to z_c-, \end{cases} \tag{3.10}$$

where

$$\left.\begin{matrix}\alpha_1 \\ \alpha_2\end{matrix}\right\} = -\frac{1}{2} \pm \left(\frac{1}{4} - r\right)^{1/2} = -\frac{1}{2} \pm m, \qquad \text{say}, \tag{3.11}$$

are the roots of

$$\alpha(\alpha + 1) + r = 0, \tag{3.12}$$

and

$$r = \frac{k^2 R}{F_c'^2}. \tag{3.13}$$

The singularity (3.10) is removed by an "inner layer", of thickness $|s_0^{1/2}/F_c'|$, surrounding, $z = z_c$.

To determine s_0 it is required to express A_1^- and A_2^- as linear combinations of A_1^+ and A_2^+, in order to be able to discover how solutions of (3.9) "pass through" the critical point. For this purpose it is necessary to solve the critical layer equation that governs the "inner solution". This problem is considered in Appendix A, where it is shown that the configuration is unstable if m is imaginary, i.e. if

$$r > r_c, \qquad \text{where} \qquad r_c = \tfrac{1}{4}; \tag{3.14, 3.15}$$

It is also shown that

$$s_0 = O\left(\exp\left[-2\pi(r - \tfrac{1}{4})^{-1/2}\right]\right), \qquad \text{as} \qquad r \to \tfrac{1}{4}. \tag{3.16}$$

The layer is, however, resistively unstable when $r < \frac{1}{4}$, as will be shown in the next Section, where the quite different critical layer equation that arises when $\Lambda \neq \infty$ (but $\Lambda \gg 1$) is investigated. It may be seen that, since F is proportional to k, r is independent of k. For example, for model (1.2) we have

$$r = \frac{R}{q^2} \qquad \text{i.e.} \qquad R_c = \tfrac{1}{4}q^2. \tag{3.17}$$

[3]The fact that (3.9) can be transformed for model (1.2) into Legendre's equation is not generally helpful, since its solutions in the ranges of interest to us have not been tabulated. One case, in which the Legendre functions simplify, is considered in Appendix A

Condition (3.14) holds for all k, even for $k \gg 1$. This is not true in case (a), for which R_c is k-dependent. [In the case $k \gg 1$, see (3.24) below.]

Table 2 shows s_0 as a function of R for one instance of case (b), namely $q = \frac{3}{2}\pi$, $k_x = k_y = 4$, in which the critical level is the mid-plane, $z_0 = \frac{1}{2}$. According to (3.17), $R_c \approx 5.5517$. The exponential dependence of s_0 shown in (3.16) makes it very difficult to find solutions numerically when R is near R_c, but the results shown are clearly consistent with (3.14). Inequality (3.8) is again obeyed.

Finally, we consider the limit $k \to \infty$, first in case (a). We restrict attention to R in the neighborhood of R_c; more precisely, we suppose that $|R/R_c - 1| \ll 1$. As already noted, $F^2_{\min}$ arises either at $z = 0$ or $z = 1$; let us suppose the former. The eigenfunction is negligibly small everywhere in $0 < z < 1$ compared with its values in a thin boundary layer, of thickness $\epsilon = O(k^{-4/3})$, on $z = 0$. Within this layer we may therefore write

$$F^2 = F^2_{\min} + 2F_{\min}F'_{\min}z\,, \tag{3.18}$$

and to leading order (3.1) becomes Airy's equation

$$\frac{d^2v_z(\xi)}{d\xi^2} = \xi v_z(\xi)\,, \tag{3.19}$$

where ξ is the stretched coordinate,

$$\xi = (z - z_0)/\epsilon\,, \tag{3.20}$$

and

$$\epsilon = \left[\frac{1}{2F_{\min}|F'_{\min}|k^2}\left(F^2_{\min} + \frac{s_0^2}{F^2_{\min}}\right)\right]^{1/3}, \qquad z_0 = \frac{R - F^2_{\min}}{2F_{\min}|F'_{\min}|}\,, \tag{3.21}$$

Since v_z must vanish outside the boundary layer, we must chose the Airy function solution of (3.19):

$$v_z(\xi) = \mathrm{Ai}(\xi)\,, \tag{3.22}$$

and to satisfy the first of (3.2) we must take

$$\epsilon\xi_0 = z_0\,, \tag{3.23}$$

where $-\xi_0$ is one of the zeros of $\mathrm{Ai}(\xi)$, all of which are negative. From (3.21) and (3.23), we obtain

$$s_0^2 = \frac{k^2}{4\xi_0^3 {F'_{\min}}^2}(R - F^2_{\min})^3 - F^4_{\min}\,, \tag{3.24}$$

which implies that

$$R_c = F^2_{\min} + \left(\frac{2}{k}\right)^{2/3}\xi_0 F^{4/3}_{\min}\left({F'_{\min}}^2\right)^{1/3}. \tag{3.25}$$

In case (b), R_c is independent of k, as noted above. It is easily seen that, for moderate R, such that $|s_0| = o(|F_c'|/k)^2$, the inner layer mentioned above (and considered in greater depth in Appendix A) is contained within an outer layer, of thickness $O(k^{-1})$, in which v_z is governed to leading order by (3.9); since $k \gg 1$, solutions to (3.9) are no longer spread out over the interval and we may replace F by $F_c'(z - z_c)$ in (3.9), so obtaining the modified spherical Bessel equation:

$$D[(z - z_c)^2 Dv_z] - [k^2(z - z_c)^2 + m^2 - \tfrac{1}{4}] v_z = 0. \tag{3.26}$$

Since solutions must vanish away from the outer layer, we must select K_m, the modified Bessel functions of the second kind, in solving (3.26):

$$v_z = \begin{cases} C^+(z - z_c)^{-1/2} K_m(k(z - z_c)), & z > z_c, \\ C^-(z_c - z)^{-1/2} K_m(k(z_c - z)), & z < z_c. \end{cases} \tag{3.27}$$

By using standard expansions of K_m about the origin, we can recover (3.11) from (3.27), and can evaluate the four constants appearing in (3.11) in terms of constants C^+ and C^-.

4. Fast and Slow g-modes

We now focus attention on solutions of the full sixth-order system (2.9) – (2.14) for the particular model (1.2) in which (2.18) holds. We shall be particularly interested in the limit $\Lambda \to \infty$, and will confine attention almost completely to cases (a) and (b).

Consider first case (a). Figures 1 show s as a function of Λ in a log-log plot for $q = \frac{1}{2}\pi$, $k_x = k_y = 1$, and for (a) $R = 8.6$ and (b) $R = 8.5$, values that straddle R_c for $\Lambda = \infty$, according to the last Section. The circles mark values obtained from integrations of the full sixth-order system. The full lines are asymptotes, which in the case (a) corresponds to the unstable mode $s_0 = 0.04891$, as given in Table 1 for $\Lambda = \infty$. More surprisingly perhaps, the system is (resistively) unstable for $R = 8.5 < R_c$. Nevertheless, $s \to 0$ as $\Lambda \to \infty$, consistent with the absence of ideal instabilities for $\Lambda = \infty$. It may also be noticed that s is asymptotically proportional to Λ^{-1}; in fact, the full line in Figure 1(b) is (see below) $s \sim 1129.3\Lambda^{-1}$.

Figures 2 compare (a) v_z and (b) ω_z for unstable cases ($R = 8.6 > R_c$) obtained from the theory of Section 3 with (c) and (d), the corresponding solutions for $\Lambda = 10^6$ obtained by integration of the full equations.[4] Figures 3 make the same comparisons but for $R = 8.5 < R_c$, for which the ideal modes are purely oscillatory according to Section 3, and for which (resistive) instabilities exist for finite Λ; again Figures 3(c) and (d) were computed for $\Lambda = 10^6$. Whereas the differences between ω_z in Figures 2(b) and (d) are two small to be easily detected, those between Figures 3(b) and (d) are dramatic, and well illustrate the even qualitative differences that a small electrical resistance can make. In both Figures 2 and 3, $q = \frac{1}{2}\pi$, $k_x = k_y = 1$.

[4] Since any solution of an eigenvalue problem can be multiplied by a constant, a question of the scaling arises here. After the numerical integrations leading to Figures 2(a) and (b) had converged, the greatest numerical value taken by v_z or ω_z in $0 < z < 1$ (which here was $v_z(\frac{1}{2})$) was scaled to unity. The same scaling factor was used for all values of v_z and ω_z. The same procedure was applied to v_z and ω_z in Figures 2(c) and (d). The comparisons displayed in Figures 3, 4, 6, 7 and 9 below were also made in this way.

We now consider, for $R < R_c$ in case (a), solutions in the limit $\Lambda \to \infty$. As indicated above, we suppose that

$$s = S/\Lambda, \qquad \text{where} \qquad S = O(1). \tag{4.1}$$

By (2.11), $\omega_z = O(\Lambda^{-2})$, so that (2.9) and (2.12) give to leading order

$$v_z = \frac{i}{\Lambda F}(D^2 - k^2 - S)b_z, \tag{4.2}$$

$$[F(D^2 - k^2) - D^2F]b_z + \frac{i\Lambda Rk^2}{S}v_z = 0, \tag{4.3}$$

which imply that

$$[F(D^2 - k^2) - D^2F]b_z - \frac{Rk^2}{SF}(D^2 - k^2 - S)b_z = 0. \tag{4.4}$$

This second order system is required to obey

$$b_z(0) = b_z(1) = 0, \tag{4.5}$$

the remaining conditions (3.14) requiring boundary layers to be constructed at $z = 0$ and $z = 1$. It is easy to show that

$$\int_0^1 \left\{ |Db_z|^2 + (k^2 + S)|b_z|^2 + \frac{F(SF - D^2F)}{(Rk^2/S - F^2)}|b_z|^2 \right\} dz = 0, \tag{4.6}$$

so that if $S > 0$ then, for model (1.2),

$$S > \frac{Rk^2}{F_{\max}^2}. \tag{4.7}$$

Table 3 shows the results of numerical integrations of (4.2) and (4.3) subject to (4.5) for $q = \frac{1}{2}\pi$, $k_x = k_y = 1$. The corresponding eigenfunctions, Λv_z and b_z, for $R = 8.5$ are shown in Figure 4(a), where where they are compared with the corresponding fields (b) obtained by integrating the full sixth-order system for $\Lambda = 10^6$.

Consider next case (b). Figures 5 show s as a function of Λ in a log-log plot for $q = \frac{3}{2}\pi$, $k_x = k_y = 4$, and for (a) $r > r_c$ and (b) $r < r_c$. The circles mark values obtained from integrations of the full sixth-order system. The full lines are asymptotes, which in the case (a) corresponds to the unstable mode $s_0 = 0.38884$, as given for $R = 12$ in Table 2 for $\Lambda = \infty$. More surprisingly perhaps, the system is (resistively) unstable for $r < r_c$. Nevertheless, $s \to 0$ as $\Lambda \to \infty$, consistent with the absence of ideal instabilities for $\Lambda = \infty$. It may also be noticed that s is asymptotically proportional to $\Lambda^{-1/2}$; in fact, the full line in Figure 5(b) is (see below) $s \sim 1.6323\Lambda^{-1/2}$.

Figures 6 compare (a) v_z and (b) ω_z for $r > r_c$ as given by the theory of Section 3 with (c) and (d), the corresponding solutions for $\Lambda = 10^6$ obtained by integration of the full equations.

We now consider, for $0 < r < \frac{1}{4}$, the solutions in case (b) in the limit $\Lambda \to \infty$. Since $s \to 0$, the outer solution obeys (3.9) and (3.2) to leading order. As $z \to z_c$, it assumes the asymptotic forms (3.10) and, as in Section 3, it is required to express A_1^- and A_2^- as linear combinations of A_1^+ and A_2^+, in order to be able to discover how solutions of (3.8) "pass through" the critical point. For this purpose it is neccssary to solve the critical layer equation that governs the "inner solution", and to match its solutions to (3.10). This critical layer is resistively dominated, and all fields within it have structures completely different from those considered in Appendix A for the case $\Lambda = \infty$.

To derive the inner solution to leading order, we introduced in Part 1 the stretched coordinate ζ,

$$z = z_c + \zeta\delta, \tag{4.8}$$

where δ is the thickness of the critical layer:

$$\delta = \frac{1}{\Lambda^{1/4}|F_c'|^{1/2}}. \tag{4.9}$$

We also defined

$$p = s\Lambda\delta^2, \qquad \alpha = -\tilde{F}_c/F_c'. \tag{4.10}$$

The same transformation gives here

$$\begin{aligned} &D\left\{\frac{1}{\zeta}(D^2 - K^2 - p)\frac{1}{\zeta}D\left[\frac{1}{\zeta}(D^2 - K^2 - p)b_z\right]\right\} \\ &\quad + 2\alpha D\left[\frac{1}{\zeta^2}D\left(\frac{b_z}{\zeta}\right)\right] + \zeta(D^2 - K^2)b_z = \frac{r}{p\zeta}(D^2 - K^2 - p)b_z, \end{aligned} \tag{4.11}$$

where now $D = d/d\zeta$, and $K = k\delta$.

It is worth comparing the problem posed by (4.11) with the similar "connection problem" encountered in Part 1, which involved (4.11) with $r = 0$. Small wavelength tearing instabilities do not exist, and attention was therefore focussed in Part 1 on $k = O(1)$. In contrast, g-mode instabilities exist at all wavenumbers, even for $K \gg 1$! For the tearing mode, $K = o(1)$ and, as shown in Part 1, $p = O(\Lambda^{-1/4})$. Thus the p terms on the left-hand side of (4.11) can then be treated as perturbations. In a similar way, the term on the right-hand side of (4.11), which is nonzero for the g-modes, is a perturbation of the same order if $r = O(\Lambda^{-1/2})$. Such modes are merely tearing modes slightly modified by buoyancy. We shall not consider them here, and shall henceforward assume that $r(< \frac{1}{4})$ is $O(1)$.

Suppose first that $K = o(1)$, so that the K^2 terms can be omitted from (4.11). Solutions to (4.11) must be found that match, as $|\zeta| \to \infty$, to the outer solutions for which, by (3.10),

$$b_z \sim \begin{cases} B_1^+(z - z_c)^{\alpha_1+1} + B_2^+(z - z_c)^{\alpha_2+1}, & z \to z_c+, \\ B_1^-(z_c - z)^{\alpha_1+1} + B_2^-(z_c - z)^{\alpha_2+1}, & z \to z_c-. \end{cases} \tag{4.12}$$

[In the limit $\Lambda \to \infty$, (2.9) gives $b_z = iFv_z/s$ and (through F) b_z contains an additional power of $z - z_c$; compare (3.10) and (4.12).] The ratios, B_2^-/B_1^- and B_2^+/B_1^+, of the

constants appearing in (4.12) are determined by solving (3.9) subject to $v_z(0) = 0$ and $v_z(1) = 0$ respectively, *and are in general both O(1).* When (4.12) is expressed in terms of the inner variable, ζ, in preparation for matching to the solutions of (4.11), we obtain

$$b_z \sim \begin{cases} B_1^+ \delta^{\alpha_1+1} \zeta^{\alpha_1+1} + B_2^+ \delta^{\alpha_2+1} \zeta^{\alpha_2+1}, & \zeta \to +\infty, \\ B_1^- \delta^{\alpha_1+1} (-\zeta)^{\alpha_1+1} + B_2^- \delta^{\alpha_2+1} (-\zeta)^{\alpha_2+1}, & \zeta \to -\infty. \end{cases} \tag{4.13}$$

Since $0 < r < \frac{1}{4}$, α_1 and $\alpha_2 (< \alpha_1)$ are real, so that $\delta^{\alpha_1+1}/\delta^{\alpha_2+1} \to 0$ as $\Lambda \to \infty$. Since B_2^-/B_1^- and B_2^+/B_1^+ are both O(1), (4.13) is to leading order

$$b_z \sim \begin{cases} B_2^+ \delta^{\alpha_2+1} \zeta^{\alpha_2+1}, & \zeta \to +\infty, \\ B_2^- \delta^{\alpha_2+1} (-\zeta)^{\alpha_2+1}, & \zeta \to -\infty. \end{cases} \tag{4.14}$$

The WKBJ method shows that, for the general solution of (4.11)

$$\begin{aligned} b_z \sim a_1^+ \zeta^{\alpha_1+1} + a_2^+ \zeta^{\alpha_2+1} &+ a_3^+ e^{(1+i)\zeta^2/2\sqrt{2}} + a_4^+ e^{(1-i)\zeta^2/2\sqrt{2}} \\ &+ a_5^+ e^{-(1+i)\zeta^2/2\sqrt{2}} + a_6^+ e^{-(1-i)\zeta^2/2\sqrt{2}}, \qquad \zeta \to +\infty, \\ b_z \sim a_1^- (-\zeta)^{\alpha_1+1} + a_2^- (-\zeta)^{\alpha_2+1} &+ a_3^- e^{(1+i)\zeta^2/2\sqrt{2}} + a_4^- e^{(1-i)\zeta^2/2\sqrt{2}} \\ &+ a_5^- e^{-(1+i)\zeta^2/2\sqrt{2}} + a_6^- e^{-(1-i)\zeta^2/2\sqrt{2}}, \qquad \zeta \to -\infty. \end{aligned} \tag{4.15}$$

In order to match to (4.14), we require that

$$a_1^+ = a_3^+ = a_4^+ = a_1^- = a_3^- = a_4^- = 0. \tag{4.16}$$

These six conditions suffice to determine the eigenvalues, p, from the sixth order equation (4.11). Interestingly, the leading order growth rate is determined *entirely* by the structure of the critical layer and is totally independent of the exterior solution. It transpires that, in the limit $\Lambda \to \infty$,

$$p = \mathrm{O}(1), \qquad \text{i.e.} \qquad s = \mathrm{O}(\Lambda^{-1/2}), \qquad \text{for} \quad k = \mathrm{O}(1). \tag{4.17}$$

This agrees with the integrations of the full equations shown in Figure 5(b).

Table 4 shows the results of numerical integrations of (4.11) subject to (4.16) for $q = \frac{3}{2}\pi$, $k_x = k_y = 4$. The corresponding eigenfunctions for $R = 4$ are shown in Figures 7(a) – (d), where they are compared with the corresponding fields [(e) – (h)] obtained by integrating the full sixth-order system for $\Lambda = 10^6$. Only the right-hand portions of the eigenfunctions in the critical layer, from the critical level itself to $\zeta = 5$, are shown in Figures 7[(a) – (d)]; the abscissae are in the stretched coordinate ζ defined by (4.8) and (4.9). These eigenfunctions should be compared with the right-hand halves of the solutions near $z = \frac{1}{2}$ derived by integrating the full equations; see Figures 7(e) – (h). In these, the full z-interval is used and the neighborhood of $z = \frac{1}{2}$ is therefore highly compressed in comparison with the corresponding Figures 7(a) – (d). It is nevertheless easy to see

that the structure of the eigenfunctions is the same in each case. As noted below (2.18) — see also Part 1 — the solutions of the full equations are not symmetric about $z = \frac{1}{2}$, although the critical layer solutions are symmetric about $\zeta = 0$. The lack of symmetry about $z = \frac{1}{2}$ is particularly evident in j_z, shown in Figure 7(h).

Consider next the instabilities for $k \gg 1$. In the range $k = o(\Lambda^{1/2})$, the outer solution becomes compressed about the critical point, and is negligible except in the outer layer described at the end of Section 3. Since $k^{-1} \gg \delta$, the critical layer governed by (4.11) is then an inner layer buried within that outer region. The matching to (4.16) proceeds much as before, and the growth rate is once more determined completely by solving (4.11) with $K = 0$; (4.17) is replaced by

$$p = O(1), \qquad \text{i.e.} \qquad s = O(k\Lambda^{-1/2}), \qquad \text{for} \quad k = o(\Lambda^{1/2}). \tag{4.18}$$

Comparing this with (4.17) we see that these instabilities grow more rapidly than the $k = O(1)$ modes; moreover, s increases monotonically with k.

When $k = O(\Lambda^{1/2})$, the outer and inner layers have the same thickness [$\delta = O(k^{-1}) = O(\Lambda^{-1/2})$], and must be considered together. We may regard this as the "critical" case. The composite layer is governed by (4.11), where now $K = O(1)$. Solutions no longer behave asymptotically as in (4.14) at the "edge" of this layer; as indicated by the behavior of the Bessel functions in (3.27), v_z is exponentially small for $|\zeta| \to \infty$. This requirement again determines the eigensolution, and we have

$$p = O(1), \qquad \text{i.e.} \qquad s = O(1), \qquad \text{for} \quad k = O(\Lambda^{1/2}). \tag{4.19}$$

As k is increased further, s becomes monotonically increasing with Λ. To see this, note that, when $k > O(\Lambda^{1/2})$, the solution again develops a double structure; the critical layer becomes an inner layer embedded in an outer layer. The outer critical layer, which is of thickness $\delta_o = (k/\Lambda F_c'^2)^{1/3}$, is governed to leading order by

$$D_o\left(\frac{1}{\zeta_o^2} D_o v_z\right) = \left(\zeta_o^2 - \frac{1}{S}\right) v_z . \tag{4.20}$$

One can seek solutions to this equation that are either symmetric or antisymmetric with respect to ζ_o, but the latter have larger eigenvalues, S^{-1}. We therefore consider only the former, requiring that

$$D_o v_z(0) = 0, \qquad v_z(\infty) = 0. \tag{4.21, 4.22}$$

Here

$$\zeta_o = \frac{(z - z_c)}{\delta_o}, \qquad S = \frac{k^{2/3}\Lambda^{1/3}}{r F_c'^{4/3}} s . \tag{4.23, 4.24}$$

Condition (4.21) eliminates the solution of (4.20) that is odd in ζ_o; (4.22) eliminates the solution of (4.20) that grows as $\exp\frac{1}{3}|\zeta_o|^3$ as $|\zeta_o| \to \infty$. Conditions (4.21) and (4.22) thus turn (4.20) into an eigenvalue problem for the scaled growth rate, S. In this way, the outer critical layer determines s without reference to the inner critical layer, which is of

thickness $\delta_i = k^{-1}$, and which merely serves to eliminate the singularity of ω_z implied by (4.20) as $|\zeta_o| \to 0$. We see from (4.24) that

$$s = O((k^2/\Lambda)^{1/3}), \qquad \text{for} \qquad k > O(\Lambda^{1/2}). \tag{4.25}$$

Figures 8 show s as functions of Λ in log-log plots for $q = \frac{3}{2}\pi$, and $R = 0.5$, and for (a) $k_x = k_y = \Lambda^{1/4}$, (b) $k_x = k_y = \Lambda^{1/2}$, and for (c) $k_x = k_y = \Lambda^{3/4}$. The circles mark values obtained from integrations of the full sixth-order system and the full lines are the asymptotes. The latter were obtained by integrating the critical layer equations: (4.11) with $K = 0$ in case (a), (4.11) with $K = O(1)$ in case (b), and (4.20) in case (c); see the entries for $R = 0.5$ in Tables 5 and 6. It is only in the case of Figure 8(c) that the agreement between the asymptotic and full solutions is not very close. This is because the fractional error made in deriving s from (4.20) – (4.24) is comparatively large, namely $O(\Lambda^{2/3}k^{-4/3})$, or $O(\Lambda^{-1/3})$ in this case. The eigenfunctions are shown for the critical case $k_x = k_y = \Lambda^{1/2}$ in Figures 9(a) – (d), where they are compared with the corresponding fields [(e) – (h)] obtained by integrating the full sixth-order system for $\Lambda = 10^5$. Only the right-hand portions of the eigenfunctions in the critical layer, from the critical level itself to $\zeta = 5$, are shown in Figures 9[(a) – (d)]; the abscissae are in the stretched coordinate ζ defined by (4.8) and (4.9). These eigenfunctions should be compared with the right-hand halves of the solutions near $z = \frac{1}{2}$ derived by integrating the full equations; see Figures 9(e) – (h). In these, only a z-interval near $z = \frac{1}{2}$ is used, the eigenfunctions being essentially zero elsewhere; the neighborhood of $z = \frac{1}{2}$ is still somewhat compressed in comparison with the corresponding Figures 9(a) – (d). It is easy to see that the structure of the eigenfunctions is the same in each case.

The tearing modes draw their energy from the magnetic energy stored in $\mathbf{B}_0$, but this energy can be released only by field line reconnection in critical layers. Not surprisingly, it was found in Part 1 that s depends strongly on the number of critical levels, and is for instance much larger in case (c) than in case (b). Although the magnetic field assists the resistive g-modes, as can be seen for example by comparing the asymptotic forms (4.1) and (4.17), it is far less influential. When $\Lambda \gg 1$, the growth rate is determined totally by the solution structure in the critical layers, and this structure is determined by r alone, which is the same for every critical layer present. Thus, in the limit $\Lambda \to \infty$, s is unaffected by the number of critical levels. This conclusion was also tested by direct integration of the full equations. Results for cases (b) and (c) are compared for the same R and k in Table 6.

5. Overstable modes.

For the purposes of argument, suppose that $\mathbf{k}$ and Λ are fixed. The layer is unstable for all sufficiently large R. It is also clear that, if R is sufficiently large and negative, the stratification will allow the propagation of MHD gravity waves, so that s will be almost

imaginary ($\approx \pm\omega$, say). In fact, the ideal equation (3.1) gives[5]

$$\begin{aligned} \omega_0 &= O(k^2(-R)^{1/2}), \qquad \text{for} \qquad R \to -\infty, \\ s_0 &= O(k^2 R^{1/2}), \qquad \text{for} \qquad R \to +\infty, \end{aligned} \tag{5.1}$$

with the same constant of proportionality in the two cases. When $\Lambda \neq 0$, the gravity waves are lightly damped by electrical resistance, i.e. $\Re s$ is small and negative for large negative R. Between $R = +\infty$ and $R = -\infty$, a transition from instability to stability must occur. As noted below (2.13), such a transition can only be direct when it occurs at $R = 0$; in all other cases it must take place via an oscillatory mode ($\Im s \neq 0$) that passes from overstability ($\Re s > 0$) to a damped oscillation as R decreases. But we know from Part 1 that, in case (b) when $k < q$ and Λ exceeds a certain critical value Λ_c, the layer is unstable to a direct tearing instability, i.e. $s > 0$ when $R = 0$. In such a situation, both direct modes *and overstable modes* must exist when $R < 0$. In all other cases the transition from instability must occur at $R = 0$ as a direct mode.

Table 7 summarizes the results of some numerical integrations performed for $k_x = k_y = 1$ and $q = \frac{3}{2}\pi$; in this case $\Lambda_c \approx 343.92$, according to Part 1. It will be seen from the table that overstability does occur before the system stabilizes.

6. Final Remarks.[6]

One may regard g-modes as complicated types of Rayleigh-Taylor ("RT") instabilities, i.e. the instabilities that arise when a lighter fluid is accelerated into a denser one, or to which a top-heavy layer of fluid in hydrostatic equilibrium is prone. The study of such instabilities has a long history during which the influences of magnetic fields and rotation have separately been investigated. An account of researches up to 1960 is given in Chapter X of Chandrasekhar (1961).

As for any other RT instability, the g-mode problem is poorly posed mathematically in the sense that every mode is unstable in the limit $k \to \infty$, i.e. no matter how short its wavelength. This difficulty is not serious; it is easily overcome by making the problem more physically realistic. By restoring the diffusivity of C unavoidable in physical reality, all modes of sufficiently small wavelength are stabilized. This is also provides a mechanism for quenching the fast g-mode instabilities and explains why, despite their large growth rate, they are not the modes of greatest interest. We plan to report on the influence of C diffusion in a future communication. We may note that short wavelength instabilities provide the basic mechanism for the model of core turbulence recently proposed by Braginsky and Meytlis (1990), and that the present paper has some implications for their theory, which we also hope to report at a later date.

The material in Chandrasekhar (1961) relevant to the present study may be summarized in the following way. When $\mathbf{B}_0 = 0$ and $\mathbf{\Omega} = 0$, instabilities exist at all wavelengths:

[5] This result holds in both cases (a) *and* (b) since, when $-R$ is sufficiently large, the real critical points defined by (3.3) lie outside $0 \leq z \leq 1$. In the limit $|R| \to \infty$, the terms proportional to F^2 in (3.1) may be neglected, and the resulting equation solved in terms of Mathieu functions. The boundary conditions (3.2) determine the eigenvalue $s_0^2 q^2/k^4 R$ or $\omega^2 q^2/k^4(-R)$, depending on whether the limit $R \to +\infty$ or $R \to -\infty$ is considered.

[6] In this Section, we abandon dimensionless fields, and revert to physical variables.

$s > 0$ for all k. In fact, ignoring viscosity and adopting the Boussinesq approximation we have, for the most unstable mode of wavenumber k,

$$(s\tau_g)^2 = \frac{(kd)^2}{\pi^2 + (kd)^2}. \tag{6.1}$$

The shorter its wavelength, the more rapidly the instability grows, but its growth rate approaches an upper bound:

$$s \to \frac{1}{\tau_g}, \qquad \text{as} \qquad k \to \infty. \tag{6.2}$$

The presence of a vertical $\mathbf{B}_0$ imparts magnetic rigidity to the layer. When $\eta = 0$ (as we temporarily suppose), lines of force are attached to fluid elements (Alfvén's theorem) and are in Faraday-Maxwell tension. Thus, $\mathbf{B}_0$ imparts magnetic rigidity to the layer. Overturning is prevented unless β and k are large enough. Instability is possible only if

$$R > \pi^2, \tag{6.3}$$

(corresponding to $k \to \infty$) but, even when this is satisfied, instability occurs only for

$$(kd)^2 > \frac{\pi^4}{R - \pi^2}. \tag{6.4}$$

The upper bound on the growth rate again occurs at vanishingly small wavelengths, but (6.2) is replaced by

$$s \to \frac{1}{\tau_g}\left(1 - \frac{\pi^2}{R}\right)^{1/2}, \qquad \text{as} \qquad k \to \infty. \tag{6.5}$$

The addition of rotation about the vertical does not affect criteria (6.3) and (6.4) for instability, nor does it alter the limit (6.5). It does however generally lengthen the time scales of the modes.

The magnetostrophic approximation used in this paper is valid for disturbances whose timescales are large compared with the Alfvén timescale,

$$\tau_A = d/V_A. \tag{6.6}$$

We have here supposed that

$$V_A/2\Omega d \ll 1, \tag{6.7}$$

so that the magnetostrophic approximation is valid for instabilities that evolve on the slow MHD timescale, $\tau_s = 2\Omega d^2/V_A^2$, but fails for inertial phenomena and also when the buoyancy timescale is too short, as happens when $\tau_g \ll d/V_A$, i.e. $R \gg 1$. Further, it gives incorrect results when k is too large. Nevertheless, near onset the instability grows slowly, so that $|s| \ll \tau_A^{-1}$. The magnetostrophic approximation therefore gives (6.3) and (6.4) correctly, although (6.5) is not recovered.

When $\mathbf{B}_0$ is horizontal rather than vertical, horizontal isotropy is lost: the direction of the wave vector $\mathbf{k}$ of the mode is significant. If $\mathbf{k}\cdot\mathbf{B}_0 = 0$ and $\Omega = 0$, results (6.1) and (6.2) again apply: Lorentz forces are not invoked and the instability grows at the same rate as in the field-free case (Chandrasekhar, 1961, §97). In contrast, when $\mathbf{k}$ and $\mathbf{B}_0$ are parallel (and $\Omega = 0$), the field stabilizes the layer in much the same way as the vertical field did. In short, for preference, the fluid overcomes the rigidity of $\mathbf{B}_0$ by overturning in rolls parallel to $\mathbf{B}_0$; the lines of magnetic force are then "interchanged" without bending and the concomitant expenditure of energy. It is worth observing that, although the interchange modes are also unstable for $R > R_c$ when $\Omega \neq 0$, they are not then the most unstable modes, i.e. the modes with the largest growth rate. Rolls orientated at other angles, $\psi = \cos^{-1}[\mathbf{k}\cdot\mathbf{B}_0/kB_0]$, to the field can make use of the Lorentz force to offset the constraint of the Coriolis force, and so release gravitational energy more rapidly. The optimum angle is given by $\cos\psi = R/\sqrt{\{2[(kd)^2 + \pi^2]\}}$.

Turning now from the well-studied situations of unidirectional $\mathbf{B}_0$ to our configuration of sheared $\mathbf{B}_0$, we may note at the outset that the equations controlling the g-mode for the sheared field are identical to those governing the field-gradient instability of a unidirectional field, i.e. a field of varying strength, F, but fixed direction. It is not surprising therefore that our case (a), in which $\mathbf{k}\cdot\mathbf{B}_0$ is nonzero throughout the layer, has stability characteristics similar to those of a unidirectional $\mathbf{B}_0$. There are, however, some crucial differences connected with the varying direction of $\mathbf{B}_0$ in the sheet pinch. For example, in our case (b) there are regions, the critical layers, in which $\mathbf{k}\cdot\mathbf{B}_0$ is very small and in which the magnetic field scarcely stabilizes the configuration. In these regions, the mode interchanges the field lines almost without bending them. At finite k, any nascent instability generated within a critical layer is required also to overcome the magnetic rigidity of the regions surrounding the critical layer in which $\mathbf{B}$ and $\mathbf{k}$ are not parallel. This inhibits the growth of the instability. The shorter the wavelength of the disturbance however, the less the fluid beyond the critical levels is involved in the motion, and the more rapidly the instability can develop.

We now turn to the effect of magnetic diffusion first for the case of horizontal $\mathbf{B}_0$ when $\mathbf{k}\cdot\mathbf{B}_0 \neq 0$. We indicated above why, when $\eta = 0$, the rigidity of $\mathbf{B}_0$ could prevent instability unless β crosses a certain threshhold value. That rigidity depended on the attachment of the field lines to the fluid elements (Alfvén's theorem). When $\eta \neq 0$, a relative motion between fluid elements and field lines beomes possible, at a rate that increases with τ_η^{-1}. Thus, the fluid can byepass the rigidity of the field lines by drifting through them. In short, instability occurs even for $R < R_c$, but its growthrate is then diffusively controlled and vanishes in the limit $\eta \to 0$, i.e. a "resistive" instability exists.

The situation for our case of sheared $\mathbf{B}_0$ is similar. The resistive instabilies of case (a) are similar to those that arise when $\mathbf{B}_0$ is vertical; those of case (b) resemble those occuring when $\mathbf{B}_0$ is horizontal and $\mathbf{k}\cdot\mathbf{B}_0 = 0$. The critical layer again controls the resistive instabilities that now arise for all $R > 0$. When R is small, the instabilities resemble the tearing modes that arise, when Λ is large enough, even in an unstratified layer ($R = 0$). These have no parallel in the case of unidirectional $\mathbf{B}_0$. Their existence guarantees that instabilities (sometimes overstabilities) will occur even for bottom-heavy stratifications.

Finally, the reason why R_c is independent of k in case (b) is of some interest. Instead of integrating (3.1) across the entire layer, as we did to deduce (3.4), let us integrate it from from 0 to z, so obtaining

$$\int_0^z \left\{ \left[F^2 + \frac{(2\Omega\mu\rho_0 s)^2}{F^2} \right] |Dv_z|^2 + k^2(F^2 - g\mu\beta)|v_z|^2 \right\} dz = \left[F^2 + \frac{(2\Omega\mu\rho_0 s)^2}{F^2} \right] v_z^* Dv_z \,. \tag{6.8}$$

Consider the case in which $R \to +R_c$, so that $s \to 0$; see Appendix A. The terms proportional to F^{-2} in (6.8) are negligible except at a critical level, $z = z_c$. Thus, if $z < z_0$ and $z_0 - z > \epsilon d$, where $\epsilon = s_0^{1/2}/|F_c'|$, we have in place of (6.8)

$$\int_0^z \left[F^2|Dv_z|^2 + k^2(F^2 - g\mu\beta)|v_z|^2 \right] dz = F^2 v_z^* Dv_z \,, \tag{6.9}$$

as can also be obtained from (3.9), which governs the outer solution to leading order. Since $|v_z| \to \infty$ as $z \to z_c$, (6.9) gives dominantly in that limit

$$\int_0^z \left[F_c'^2 (z_c - z)^2 |Dv_z|^2 - k^2 g\mu\beta |v_z|^2 \right] dz = F^2 v_z^* Dv_z \,. \tag{6.10}$$

The infinite contribution from the gravitational term must be balanced by equal contributions from the magnetic term, so that $F_c'^2(z_c - z)^2|Dv_z|^2$ must be of order $k^2 g\mu\beta|v_z|^2$, i.e. v_z must be $O(z_c - z)^{-1/2}$. The dominant contributions then cancel if $\frac{1}{4}F_c'^2 = k^2 g\mu\beta$, which is equivalent to criterion (3.14). Since F is proportional to k, R_c is independent of k.

Acknowledgements. One of us (WK) is grateful to the National Science Foundation for support under grant EAR–8846267; the other of us (PHR) thanks NSF for the same reason, and also thanks the Office of Naval Research for partial support under a URI grant N00014-86-0641. He is also grateful to our colleague, Dr. Charles Lange, for a useful discussion.

References

Abramowitz, M. and Stegun, I.A. (Eds.), *Handbook of Mathematical Functions with Formulas, Graphs, and Mathematical Tables*, National Bureau of Standards, Applied Mathematics Series 55 (1964).

Braginsky, S.I. "Magnetohydrodynamic waves within the Earth", pp.733-740 in *The Encylopedia of Solid Earth Geophysics*, ed. David E. James, New YorK: van Nostrand Reinhold Co. (1989).

Braginsky, S.I. and Meytlis, V.P. "Local turbulence in the Earth's core", *Geophys. & Astrophys. Fluid Dynam.*, **55**, 71–88 (1990).

Chandrasekhar, S. *Hydrodynamic and Hydromagnetic Stability*, University Press, Oxford (1961).

Fearn, D.R. "Differential rotation and thermal convection in a rapidly rotating hydromagnetic system," *Geophys. Astrophys. Fluid Dynam.* **49**, 173–193 (1989).

Furth, H.P., Killeen, J. and Rosenbluth, M.N. "Finite resistive instabilities of a sheet pinch," *Phys. Fluids* **6**, 459–484 (1963).

Kuang, W. and Roberts, P.H. "Resistive instabilities in rapidly rotating fluids: linear theory of the tearing mode," *Geophys. & Astrophys. Fluid Dynam.*, **55**, 183-223 (1990).

APPENDIX A: MARGINALLY UNSTABLE IDEAL MODES

The objective of this appendix is to extend the analysis of Section 3 by finding the growth rate, s_0 of the unstable ideal modes in case (b) in the limit $\mu \rightarrow +0$, where

$$\mu^2 = r - \tfrac{1}{4}; \tag{A1}$$

in this limit $s_0 \rightarrow +0$. The solution consists of outer regions, asymptotically excluding both the critical layer surrounding $z = z_c$ and the two boundary layers on $z = 0$ and $z = 1$. The latter are passive, i.e. do not affect the outer solution or s_0 to leading order; they will be considered no further here.

The leading order asymptotic problem is that of solving (3.9) twice, once for $0 \leq z < z_c$ and once for $z_c < z \leq 1$. Each solution must satisfy whichever of (3.2) lies in its interval. When the resulting solutions are expanded for $z \rightarrow z_c$, expressions of the form (3.11) are recovered with

$$m = i\mu. \tag{A2}$$

In this appendix we shall write

$$A_1^{\pm} = -iA^{\pm}\exp\left(i\mu\delta^{\pm}\right) = A_2^{\pm *}, \tag{A3}$$

where the phases $\delta^{\pm}$ are determined by (3.1) and (3.2). The phase difference between A_1^+ and $-A_2^+$, and similarly between A_1^- and $-A_2^-$ is small for the following reason. As $\mu \rightarrow 0$, the solution in $z_c < z \leq 1$ that is asymptotically $(z - z_c)^{-\frac{1}{2}+i\mu}$ for $z \rightarrow z_c^+$ approaches the solution that is asymptotically $(z - z_c)^{-\frac{1}{2}-i\mu}$; their difference is $O(\mu)$. Thus, to satisfy the boundary condition $v_z(1) = 0$, A_2^+ must coincide with $-A_1^+$ as $\mu \rightarrow 0$; moreover, $A_2^+/A_1^+ + 1$ must be $O(\mu)$. Similar remarks apply to the solutions in $0 \leq z < z_c$. The ratio, A^+/A^-, of moduli in (A3) cannot be determined until the two solutions are connected across the critical layer. Such a connection is generally impossible, but can be brought about if μ and s_0 are related by a dispersion relationship, which reflects the eigenvalue character of the problem. It is intended to find the asymptotic form of this relationship in the limit $s_0 \rightarrow +0$.

To study the critical layer, we introduce the stretched coordinate, ζ, where

$$z - z_c = \epsilon\zeta, \qquad \text{and} \qquad \epsilon = s_0^{1/2}/|F_c'|. \tag{A4}$$

In terms of this variable, (3.10) and (A3) give

$$v_z \sim \begin{cases} 2\epsilon^{-1/2}A^+ \quad \zeta^{-1/2} \quad \sin\left[\mu\ln\zeta + \mu\delta^+ + \mu\ln\epsilon\right], & \zeta \to \infty, \\ 2\epsilon^{-1/2}A^-(-\zeta)^{-1/2}\sin\left[\mu\ln(-\zeta) + \mu\delta^- + \mu\ln\epsilon\right], & \zeta \to -\infty, \end{cases} \tag{A5}$$

On applying (A4) to (3.1), we find that in the critical layer v_z obeys, to leading order,

$$\left(1 + \zeta^4\right)\frac{d^2v_z}{d\zeta^2} - \frac{2}{\zeta}\left(1 - \zeta^4\right)\frac{dv_z}{d\zeta} + r\zeta^2 v_z = 0, \tag{A6}$$

the general solution to which is

$$v_z = a_1 v_1 + a_2 v_2, \tag{A7}$$

where a_1 and a_2 are constants,

$$v_1 = F\left(\tfrac{1}{8} + \tfrac{1}{4}i\mu, \tfrac{1}{8} - \tfrac{1}{4}i\mu; \tfrac{1}{4}; -\zeta^4\right), \tag{A8}$$

$$v_2 = \zeta^3 F\left(\tfrac{7}{8} + \tfrac{1}{4}i\mu, \tfrac{7}{8} - \tfrac{1}{4}i\mu; \tfrac{7}{4}; -\zeta^4\right), \tag{A9}$$

and F denotes the hypergeometric function; evidently v_1 is even and v_2 is odd about the critical level $\zeta = 0$:

$$v_1(-\zeta) \equiv v_1(\zeta), \qquad v_2(-\zeta) \equiv -v_2(\zeta). \tag{A10}$$

Standard theory (e.g. Abramowitz and Stegun, 1964, Eq. 15.3.7), together with (A10) provides expressions for v_1 and v_2 that are valid at the edges of the critical layer: for real ζ and $|\zeta| > 1$, we have

$$v_1 = \frac{\Gamma\left(\frac{1}{4}\right)\Gamma\left(\frac{1}{2}i\mu\right)}{\left[\Gamma\left(\frac{1}{8} + \frac{1}{4}i\mu\right)\right]^2}|\zeta|^{-\frac{1}{2}+i\mu}F\left(\tfrac{1}{8} - \tfrac{1}{4}i\mu, \tfrac{7}{8} - \tfrac{1}{4}i\mu; 1 - \tfrac{1}{2}i\mu; -\frac{1}{\zeta^4}\right) + *, \tag{A11}$$

$$v_2 = \frac{\Gamma\left(\frac{7}{4}\right)\Gamma\left(\frac{1}{2}i\mu\right)}{\left[\Gamma\left(\frac{7}{8} + \frac{1}{4}i\mu\right)\right]^2}|\zeta|^{-\frac{1}{2}+i\mu}F\left(\tfrac{1}{8} - \tfrac{1}{4}i\mu, \tfrac{7}{8} - \tfrac{1}{4}i\mu; 1 - \tfrac{1}{2}i\mu; -\frac{1}{\zeta^4}\right)\operatorname{sgn}\zeta + *, \tag{A12}$$

where the asterisk on each right-hand side denotes the complex conjugate of the expression that preceded it. For the purposes of matching to (A5), we need only the leading order parts of (A11) and (A12), namely

$$v_1 \sim \frac{4\Gamma\left(\frac{1}{4}\right)}{\mu\left[\Gamma\left(\frac{1}{8}\right)\right]^2}|\zeta|^{-1/2}\sin\left[\mu\ln|\zeta| + l_1\mu\right], \tag{A13}$$

$$v_2 \sim \frac{4\Gamma\left(\frac{7}{4}\right)}{\mu\left[\Gamma\left(\frac{7}{8}\right)\right]^2}|\zeta|^{-1/2}\sin\left[\mu\ln|\zeta| + l_2\mu\right]\operatorname{sgn}\zeta, \tag{A14}$$

where

$$l_1 = -\tfrac{1}{2}\left[\gamma + \psi\left(\tfrac{1}{8}\right)\right] \approx 3.905638318\ldots,$$
$$l_2 = -\tfrac{1}{2}\left[\gamma + \psi\left(\tfrac{7}{8}\right)\right] \approx 0.113400703\ldots.$$

Here ψ is the digamma function and $\gamma = -\psi(1)$ is Euler's constant.

In matching the inner solution to the outer solutions, we absorb the constant prefactors in (A13) and (A14) into a_1 and a_2, and multiply these constants by $2\epsilon^{1/2}$; see (A5). After these cosmetic changes, the matching conditions become

$$a_1 \sin[\mu \ln|\zeta| + l_1\mu] + a_2 \sin[\mu \ln|\zeta| + l_2\mu] = A^+ \sin\left[\mu \ln|\zeta| + \mu\delta^+ + \mu \ln\epsilon\right], \tag{A15}$$

$$a_1 \sin[\mu \ln|\zeta| + l_1\mu] - a_2 \sin[\mu \ln|\zeta| + l_2\mu] = A^- \sin\left[\mu \ln|\zeta| + \mu\delta^- + \mu \ln\epsilon\right], \tag{A16}$$

Discarding $O(\mu^2)$ terms as before, we obtain from (A15) and (A16) the dispersion relationship

$$\mu \ln\epsilon = -n\pi + \tfrac{1}{2}\mu(l_1 + l_2 - \delta^+ - \delta^- \pm \mathcal{R}), \tag{A17}$$

where n is a positive integer and

$$\mathcal{R} = +\sqrt{[(l_1 - l_2)^2 + (\delta^+ - \delta^-)^2]}. \tag{A18}$$

(Since we are concerned with the limits $\mu \to 0$ and $\ln\epsilon \to -\infty$, n cannot be negative or zero.) To obtain the most rapidly growing mode, we must take $n = 1$ and the upper sign in (A17). The required solution is therefore

$$s_0 = C\,\mathrm{e}^{-2\pi/\mu}, \tag{A19}$$

where

$$C = F_c'^2 \exp[l_1 + l_2 - \delta^+ - \delta^- + \mathcal{R}]. \tag{A20}$$

In the case of model (1.2), two independent solutions of (3.8) are

$$v_z^{(1)} = \operatorname{cosec} q(z - z_c)\, P_\beta^{\alpha_1}(\xi), \qquad v_z^{(2)} = \operatorname{cosec} q(z - z_c)\, P_\beta^{\alpha_2}(\xi), \tag{A21}$$

where

$$\xi = i \cot\left[\tfrac{1}{2}q(z - z_c)\right], \qquad \beta^2 = 1 - (k/q)^2, \tag{A22}$$

and P_β^α denotes the Legendre function. It follows that

$$v_z = \begin{cases} B^+ \dfrac{\operatorname{cosec} q(z - z_c)}{\operatorname{cosec} q(1 - z_c)} \left[\dfrac{P_\beta^{\alpha_1}(\xi)}{P_\beta^{\alpha_1}(\xi_1)} - \dfrac{P_\beta^{\alpha_2}(\xi)}{P_\beta^{\alpha_2}(\xi_1)}\right], & z_c < z \le 1, \\ B^- \dfrac{\operatorname{cosec} q(z_c - z)}{\operatorname{cosec} q z_c} \left[\dfrac{P_\beta^{\alpha_1}(-\xi)}{P_\beta^{\alpha_1}(-\xi_0)} - \dfrac{P_\beta^{\alpha_2}(-\xi)}{P_\beta^{\alpha_2}(-\xi_0)}\right], & 0 \le z < z_c, \end{cases} \tag{A23}$$

where

$$\xi_0 \;=\; \xi(0) \;=\; -i\cot\tfrac{1}{2}qz_c, \qquad\qquad \xi_1 \;=\; \xi(1) \;=\; i\cot\tfrac{1}{2}q(1-z_c)\,. \tag{A24}$$

Little useful information is available to us about P_β^α for complex α, so we consider a special case ($\beta \;=\; \frac{1}{2}$) in which such information is readily available:

$$k \;=\; \tfrac{1}{2}\sqrt{3}\,q\,. \tag{A25}$$

In place of (A23), we then have

$$v_z \;=\; \begin{cases} C^+\left[\dfrac{\sin\,q(z-z_c)}{\sin\,q(1-z_c)}\right]^{-\frac{1}{2}}\left[\left(\dfrac{\xi}{\xi_1}\right)^{-i\mu} \;-\; \left(\dfrac{\xi}{\xi_1}\right)^{i\mu}\right], & z_c < z \le 1, \\ C^-\left[\dfrac{\sin\,q(z_c-z)}{\sin\,qz_c}\right]^{-\frac{1}{2}}\left[\left(\dfrac{\xi}{\xi_0}\right)^{-i\mu} \;-\; \left(\dfrac{\xi}{\xi_0}\right)^{i\mu}\right], & 0 \le z < z_c, \end{cases} \tag{A26}$$

so that

$$\delta^+ \;=\; \ln\tfrac{1}{2}q \;-\; \ln\tan\tfrac{1}{2}q(1-z_c)\,, \qquad\qquad \delta^- \;=\; \ln\tfrac{1}{2}q \;-\; \ln\tan\tfrac{1}{2}qz_c\,.$$

Case (b) has been illustrated in this paper principally by the example $q \;=\; \frac{3}{2}\pi$, $z_c \;=\; \frac{1}{2}$, for which $\delta^+ \;=\; \delta^- \;\approx\; -0.024325773$, so that by (A20)

$$C \;=\; 958405.348\ldots. \tag{A27}$$

The fractional error in (A19) is of order μ. It is easy in the special case (A25) to derive a result in which the fractional error is only $O(s^2)$. This is the error made if one replaces the hypergeometric functions in (A11) and (A12) by unity but does not approximate the gamma functions; the $O(\zeta^{-4})$ terms omitted are $O(s^2)$ by (A4), as are the terms lost in deriving (A6). Using (A11) in place of (A13), one obtains instead of (A19)

$$s_0 \;=\; \left(F_c'\frac{\tan\frac{1}{4}q}{\frac{1}{2}q}\right)^2\left[\frac{\Gamma(1+\frac{1}{2}i\mu)}{\Gamma(1-\frac{1}{2}i\mu)}\left(\frac{\Gamma(\frac{1}{8}-\frac{1}{4}i\mu)}{\Gamma(\frac{1}{8}+\frac{1}{4}i\mu)}\right)^2\right]^{1/i\mu}. \tag{A28}$$

Values derived from (A28) are shown in Table 8, as are values of $s_0\exp(2\pi/\mu)$, which give some idea how much C would vary if (A19) were taken beyond its asymptotic validity. The asymptotic results become increasingly inaccurate as R increases from R_c. Values from numerical computation are also presented, obtained using Richardson extrapolations of integrations with a step size of $2.5\;10^{-4}$. These results become increasingly inaccurate as R is decreased towards R_c. It will be seen that there is an interval of R in which the two methods give consistent results.

TABLE 1

Ideal growth rates, s_0, for $q = \frac{1}{2}\pi$, and $k_x = k_y = 1$.

R	s_0^2	s_0
50.0	11.723	± 3.4239
30.0	5.9628	± 2.4419
14.0	1.4333	± 1.1972
10.0	0.35871	± 0.59892
8.8	0.052285	± 0.22866
8.6	0.002392	± 0.04891
8.5904...	0	0
8.5	-0.02240	$\pm 0.14968i$
6.0	-0.59518	$\pm 0.77148i$

TABLE 2

Ideal growth rates, s_0, for $q = \frac{3}{2}\pi$, and $k_x = k_y = 4$.

R	s_0^2	s_0
20.0	90.6781	± 9.5225
16.0	10.4222	± 3.2283
14.0	1.8598	± 1.3638
12.0	0.15124	± 0.3889
11.0	0.02573	± 0.1604
10.0	0.002388	± 0.0489
9.2	0.0001742	± 0.0132
8.6	0.0000122	± 0.0035
5.5517...	0.0	0.0

TABLE 3

Growth rates, s, in the limit $\Lambda \to \infty$, for $q = \frac{1}{2}\pi$, $k_x = k_y = 1$ and $R < R_c$.

R	$S = s_0\Lambda$
8.5	1129.3
8.4	529.84
8.0	162.81
7.2	62.298
5.0	16.850
3.0	6.5795
1.0	1.9875

TABLE 4

Scaled growth rates, $\Lambda^{1/2}s$, for $q = \frac{3}{2}\pi$, and $k_x = k_y = 4$ and $r < \frac{1}{4}$, both for $\Lambda \to \infty$ and $\Lambda = 10^6$.

R	For $\Lambda \to \infty$	For $\Lambda = 10^6$
0.2	0.32036	0.31995
0.5	0.80598	0.80452
0.6	0.96941	0.96746
1.0	1.6323	1.6275
2.0	3.3764	3.3530
3.0	5.3165	5.2355
4.0	7.6238	7.3617

TABLE 5

Growth rates, s, for fast g-modes in the critical case $k_x = k_y = \Lambda^{1/2}$, both for $\Lambda \to \infty$ and $\Lambda = 10^6$.
Also $q = \frac{3}{2}\pi$, and $r < \frac{1}{4}$.

R	For $\Lambda \to \infty$	For $\Lambda = 10^6$
0.2	0.067671	0.067615
0.5	0.16945	0.16934
0.6	0.20346	0.20333
1.0	0.33990	0.33976
2.0	0.68444	0.68452
3.0	1.0348	1.0355
4.0	1.3920	1.3940

TABLE 6

Growth rates, $\Lambda^{1/2}s$, of resistive g-modes when one critical level exists and when two exist.
For the former $k_x = k_y = 4$; for the latter $k_x = -k_y = 1$.
In both cases $q = \frac{3}{2}\pi$, $\Lambda = 10^6$ and $r < \frac{1}{4}$.

R	One critical level	Two critical levels
0.2	0.31995	0.31993
0.6	0.96746	0.96726
1.0	1.6275	1.6268
2.0	3.3530	3.3488
3.0	5.2355	5.2224
4.0	7.3617	7.3296
5.0	9.8741	9.8037

TABLE 7

Overstable Modes for negative R.

Growth rates, $\Re s$, and $\Im s$ are given for several Λ and R.

In each case $q = \frac{3}{2}\pi$ and $k_x = k_y = 1$.

Λ	$R \times \Lambda$	$\Re s$	$\Im s$
350	-0.02	0.0001874	0.0
	-0.03	0.0001399	$\pm$0.0000805
	-10.0	0.0000012	$\pm$0.0029460
	-10.1	-0.0000002	$\pm$0.0029607
500	-13.0	0.0021552	0.0
	-14.0	0.0021231	$\pm$0.00061864
	-28.1	0.0000047	$\pm$0.0098451
	-28.2	-0.0000032	$\pm$0.0098624
1000	-163.	0.0033593	0.0
	-164.	0.0031242	$\pm$0.00015158
	-1310.	0.0000032	$\pm$0.0086982
	-1320.	-0.0000232	$\pm$0.0087300
10000	-7051.	0.0010452	0.0
	-7052.	0.0010364	$\pm$0.000015489
	-20300.	0.0000062	$\pm$0.0016621
	-20400.	-0.0000010	$\pm$0.0016654

TABLE 8

Comparison of asymptotic theory with numerical results for the case of one critical level and small values of $r - \frac{1}{4}$.

$q = \frac{3}{2}\pi$ and $k_x = k_y = \frac{1}{2}\sqrt{3}\,q$.

R	C	asymptotic s	numerical s
5.55165...	958405.35	0.0	
5.6	936684.87	$3.0912604\ 10^{-53}$	
5.7	893978.74	$3.6750897\ 10^{-28}$	
5.8	854057.00	$1.3433167\ 10^{-20}$	
6.0	781668.30	$4.8836799\ 10^{-14}$	
6.4	661561.81	$7.2361873\ 10^{-9}$	
7.2	490890.72	$4.7347138\ 10^{-5}$	$6.\ 10^{-5}$
7.5	443482.35	$2.719511\ 10^{-4}$	$2.72\ 10^{-4}$
8.0	378437.85	$2.29058\ 10^{-3}$	$2.2908\ 10^{-3}$
8.5	326774.18	$1.06019\ 10^{-2}$	$1.0607\ 10^{-2}$
9.0	285102.48	$3.3909\ 10^{-2}$	$3.3952\ 10^{-2}$
9.5	251030.74	$8.479\ 10^{-2}$	$8.50055\ 10^{-2}$
10.0	222834.71	$1.783\ 10^{-1}$	$1.79051\ 10^{-2}$

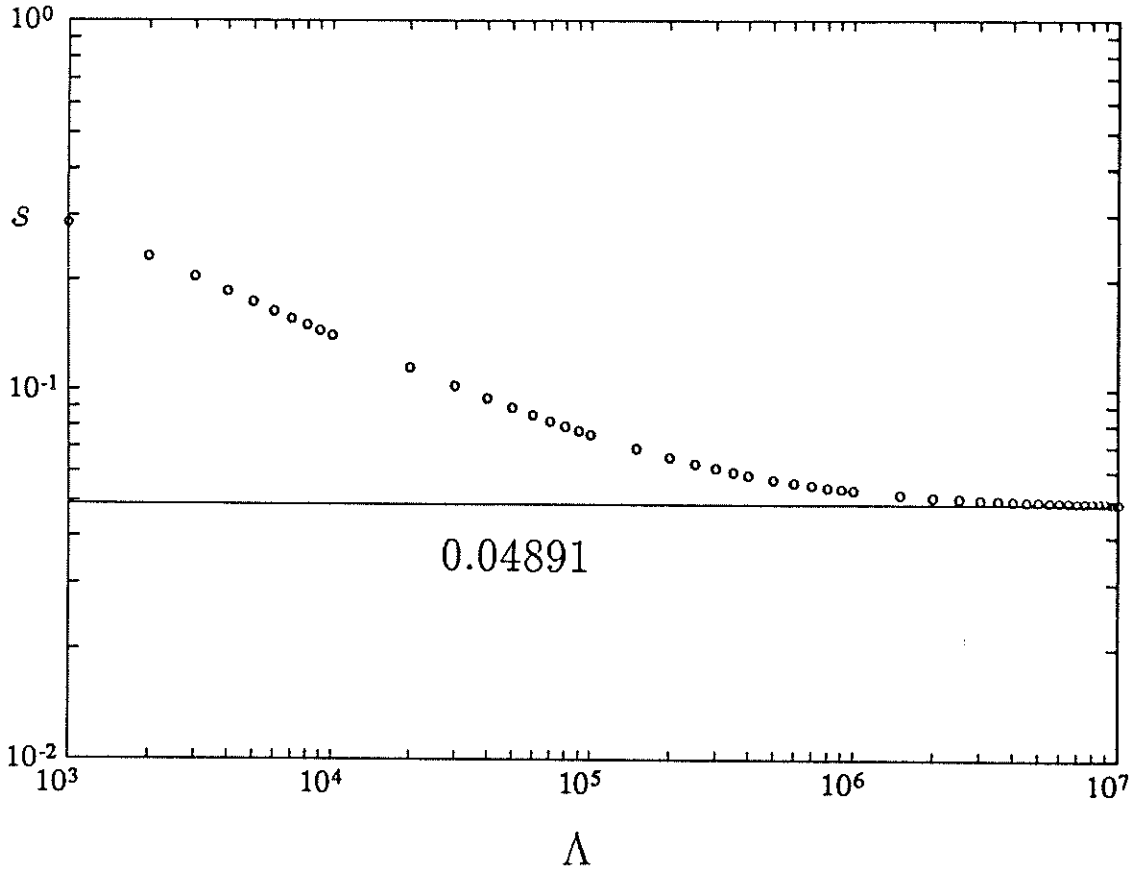

Figure 1(a). Growth rate, s, as a function of Λ in a log-log plot for a case in which there is no critical level in the layer: $k_x = k_y = 1$, $q = \frac{1}{2}\pi$ and $R = 8.6$ ($> R_c$).

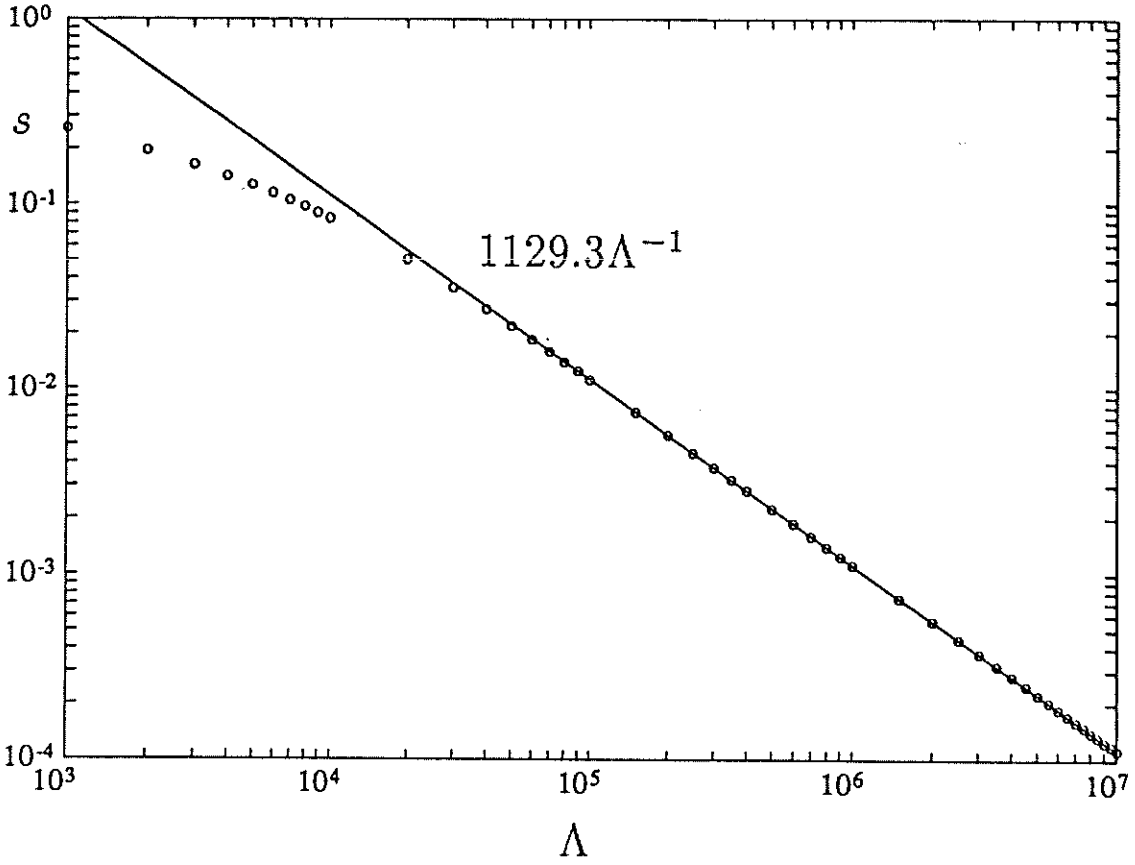

Figure 1(b). Growth rate, s, as a function of Λ in a log-log plot for a case in which there is no critical level in the layer: $k_x = k_y = 1$, $q = \frac{1}{2}\pi$ and $R = 8.5\ (< R_c)$.

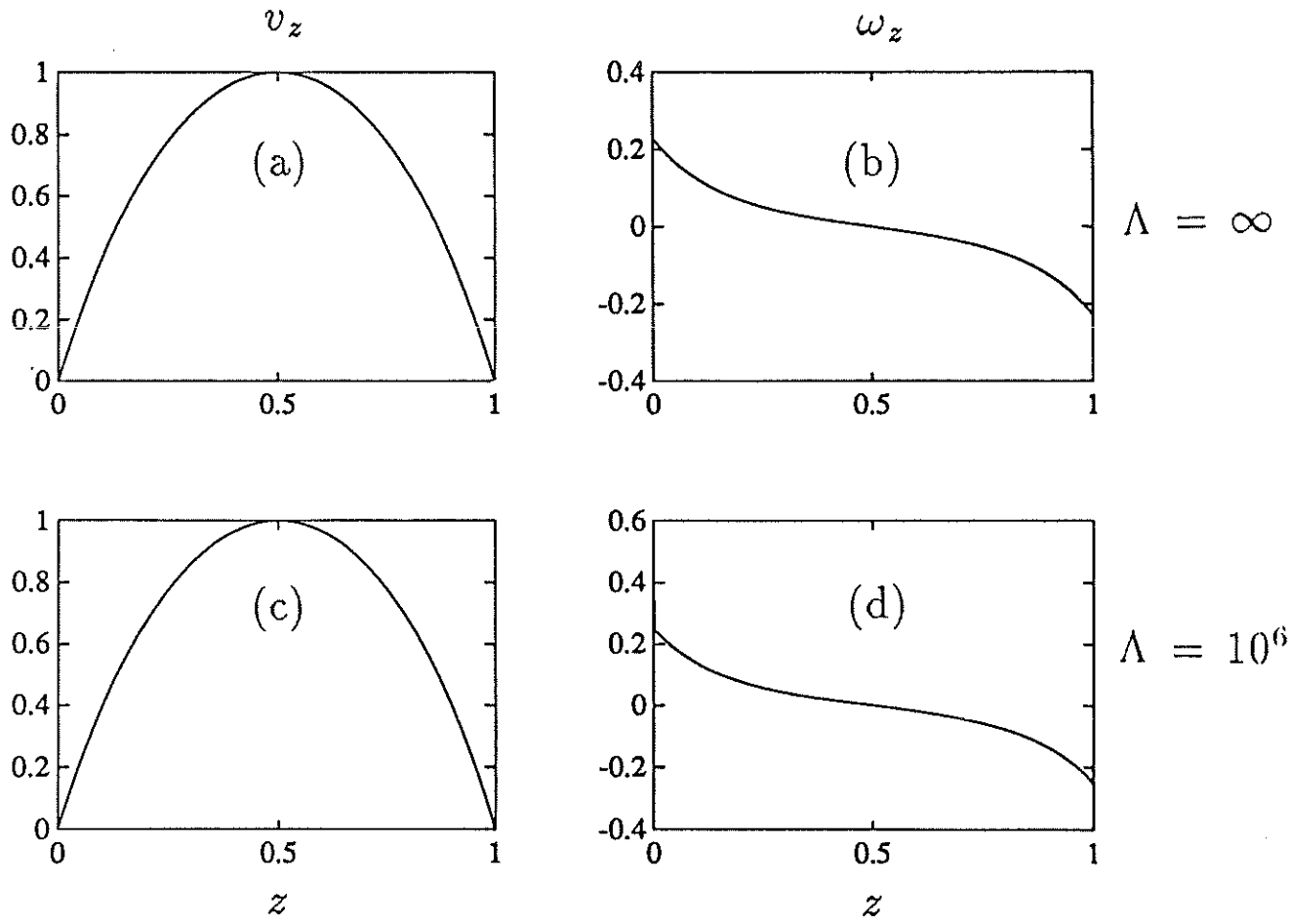

Figures 2. Comparisons between eigenfunctions for ideal instabilities ($\Lambda = \infty$) [panels (a) and (b)], and those for the corresponding instabilities for large Λ [panels (c) and (d)]. There is no critical level in the layer; in all cases $k_x = k_y = 1$, $q = \frac{1}{2}\pi$, and $R = 8.6$; in panels (c) and (d), $\Lambda = 10^6$. The velocity perturbation, v_z, is shown in panels (a) and (c) and the vorticity perturbation, ω_z, in panels (b) and (d).

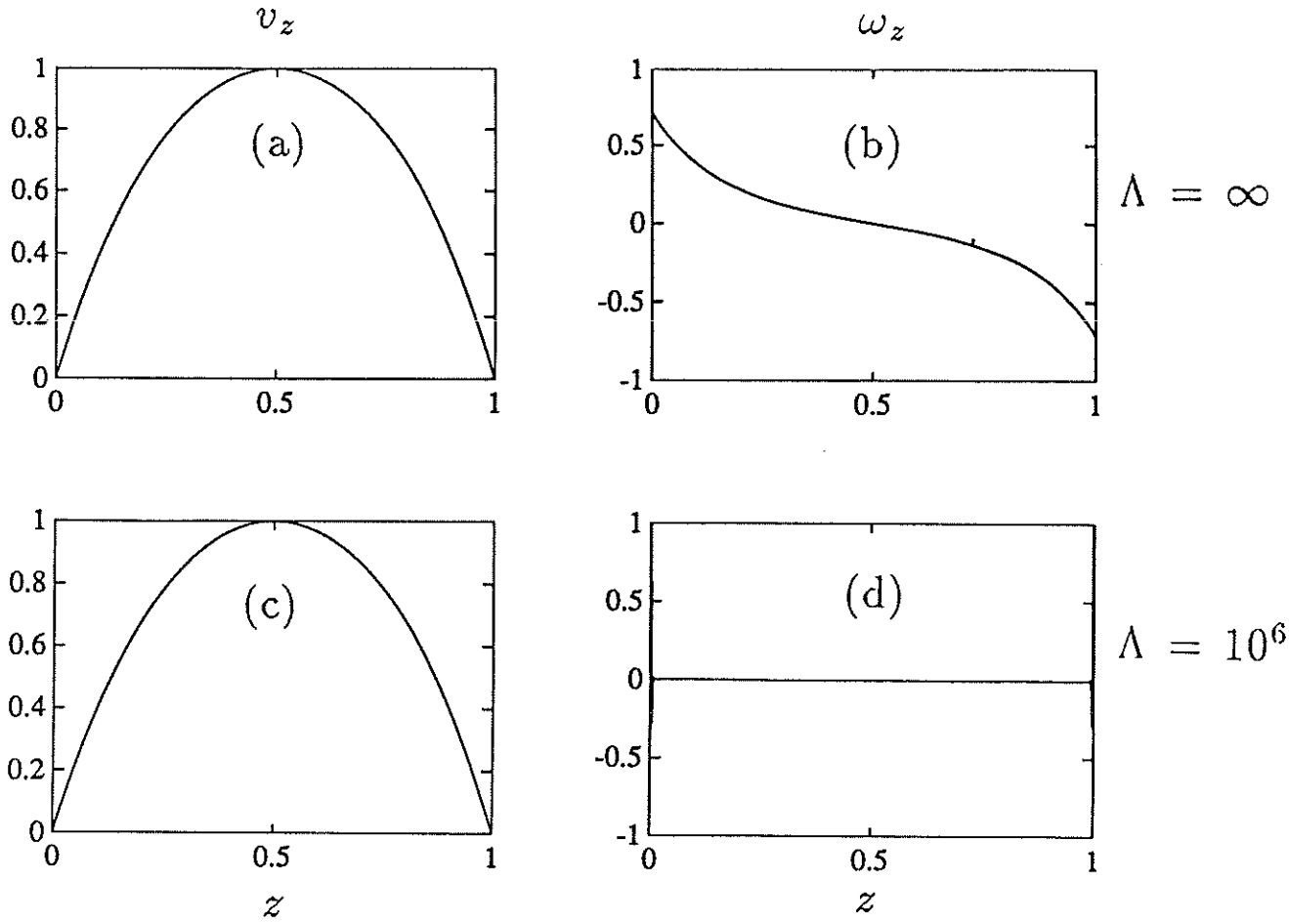

Figures 3. Comparisons between eigenfunctions for stable ideal modes ($\Lambda = \infty$) [panels (a) and (b)], and those for the corresponding resistive instabilities for large Λ [panels (c) and (d)]. There is no critical level in the layer; in all cases $k_x = k_y = 1$, $q = \frac{1}{2}\pi$, and $R = 8.5$; in (c) and (d), $\Lambda = 10^6$. The velocity perturbation, v_z, is shown in panels (a) and (c) and the vorticity perturbation, ω_z, in panels (b) and (d).

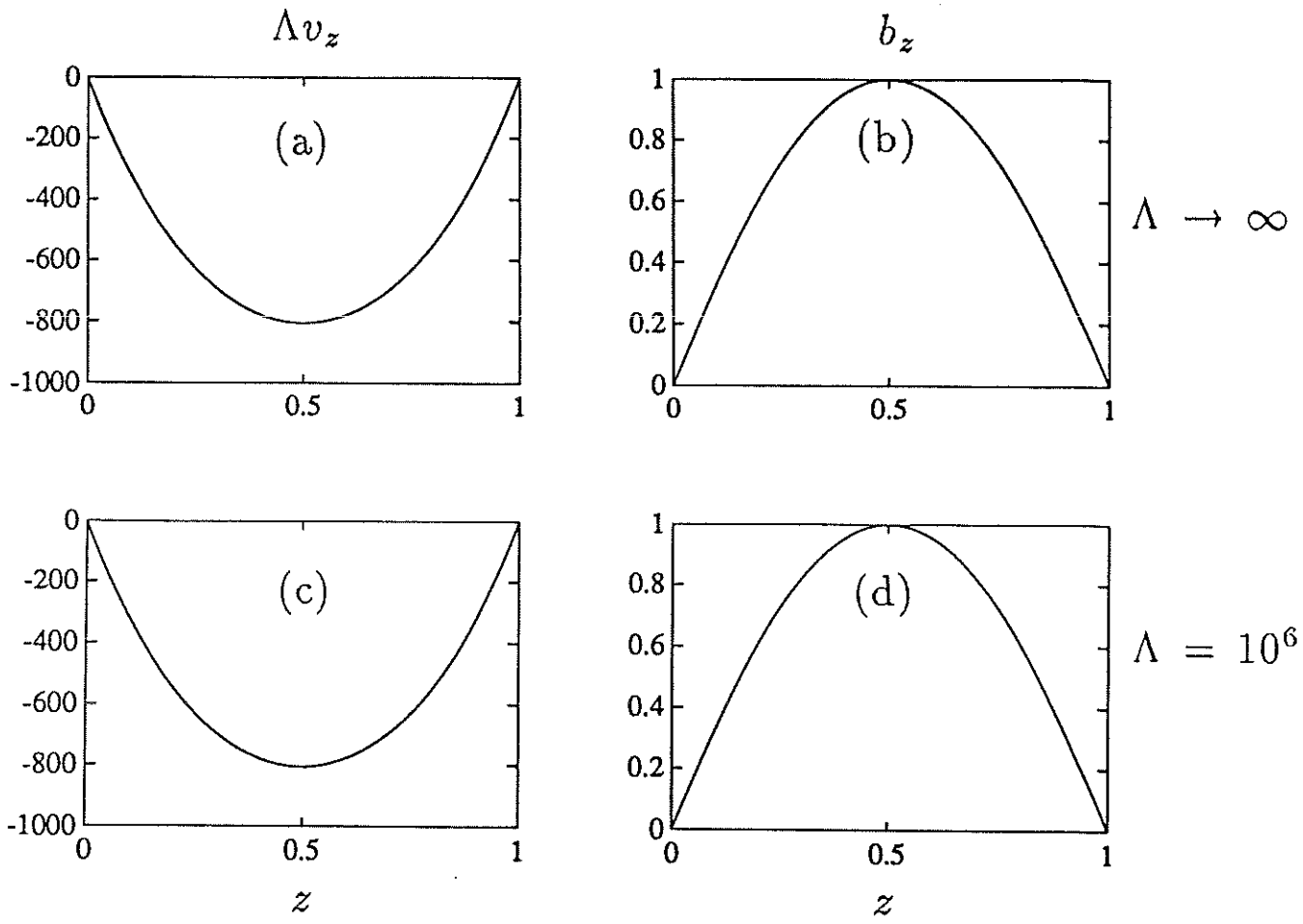

Figures 4. Comparisons between eigenfunctions for resistive instabilities in the limit of infinite Λ [panels (a) and (b)], and those for the corresponding modes for large Λ [panels (c) and (d)]. There is no critical level in the layer; in all cases $k_x = k_y = 1$, $q = \frac{1}{2}\pi$, and $R = 8.5$; in panels (c) and (d), $\Lambda = 10^6$. The scaled velocity perturbation, Λv_z, is shown in panels (a) and (c) and magnetic field perturbation, $-ib_z$ in panels (b) and (d).

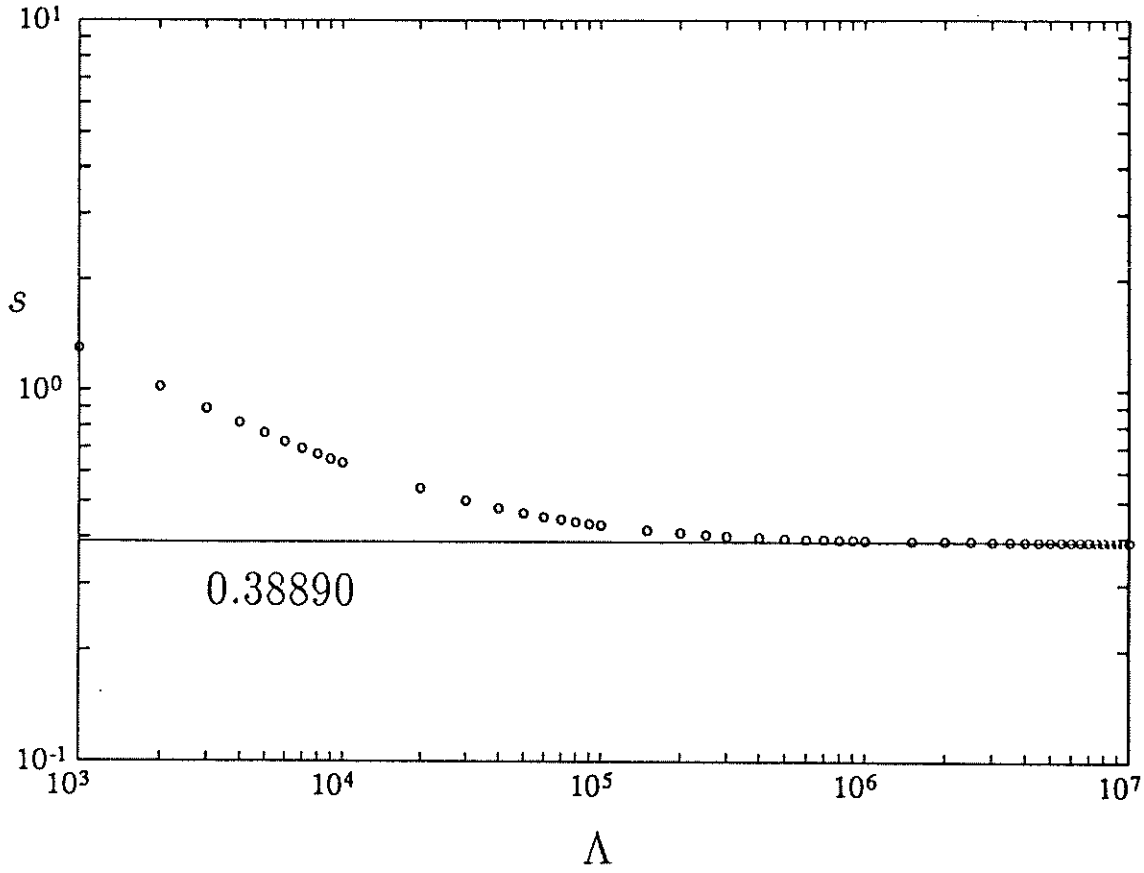

Figure 5(a). Growth rate, s, as a function of Λ in a log-log plot for a case in which there is one critical level in the layer: $k_x = k_y = 4$, $q = \frac{3}{2}\pi$ and $R = 12$ $(> R_c)$.

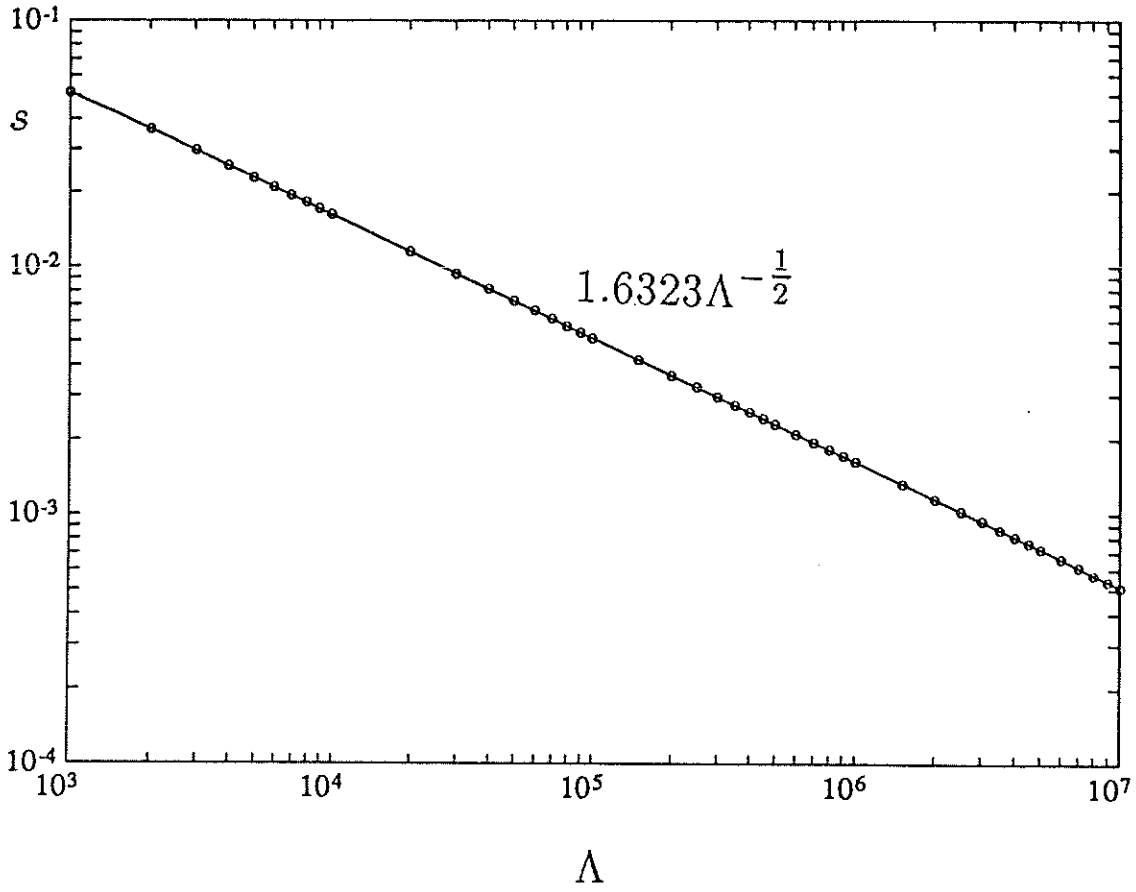

Figure 5(b). Growth rate, s, as a function of Λ in a log-log plot for a case in which there is no critical level in the layer: $k_x = k_y = 4$, $q = \frac{3}{2}\pi$ and $R = 1\ (< R_c)$.

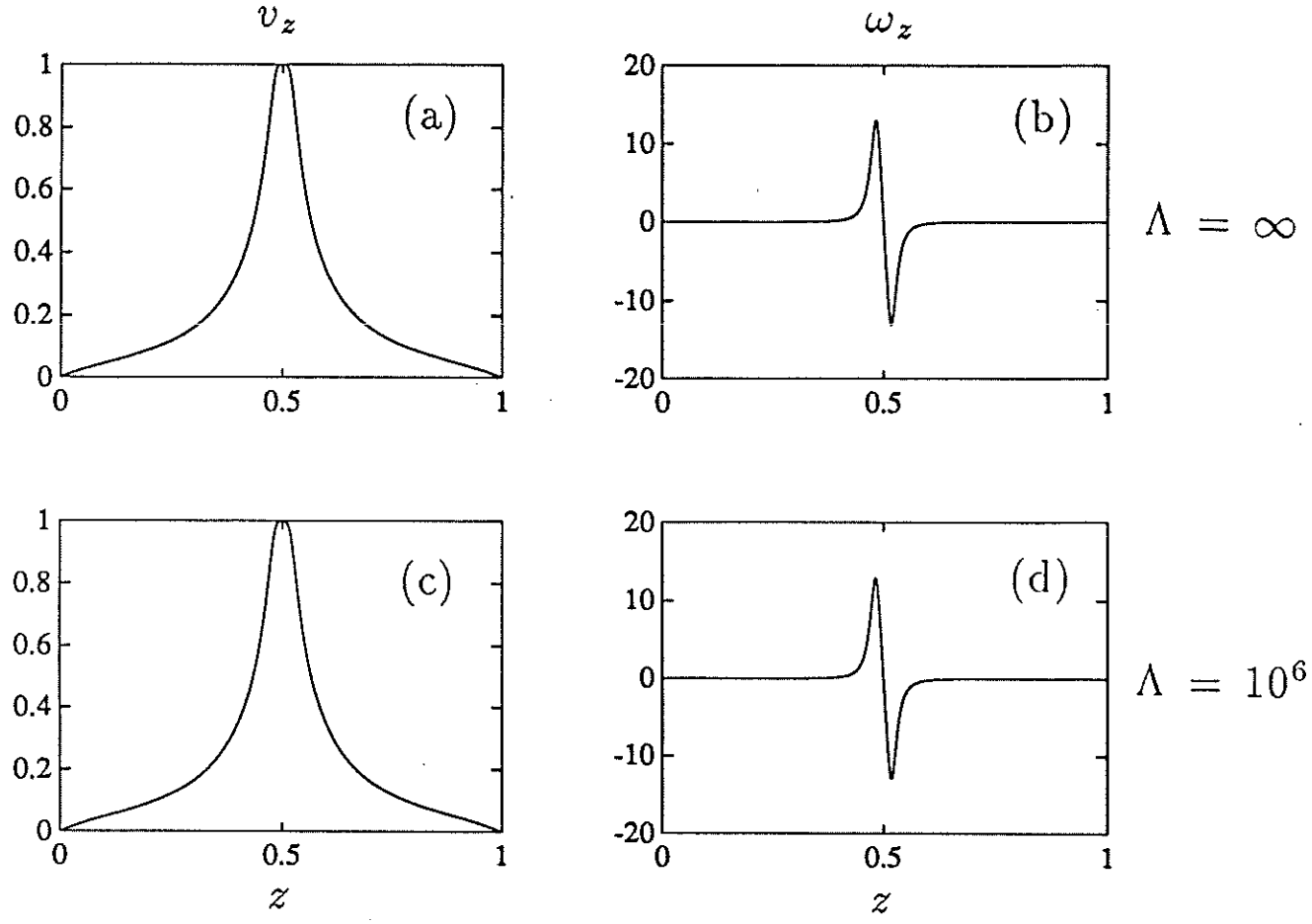

Figures 6. Comparisons between eigenfunctions for ideal instabilities ($\Lambda = \infty$) [panels (a) and (b)], and those for the corresponding instabilities for large Λ [panels (c) and (d)]. There is one critical level in the layer; in all cases $k_x = k_y = 4$, $q = \frac{3}{2}\pi$, and $R = 12$; in (c) and (d), $\Lambda = 10^6$. The velocity perturbation, v_z, is shown in panels (a) and (c) and the vorticity perturbation, ω_z, in panels (b) and (d).

For Figures 7 see following page.

Figures 7. Comparisons between the eigenfunctions [(a) – (d)] for the resisitive modes in the critical layer in the limit $\Lambda \to \infty$ with the eigenfunctions [(e) – (h)] in the entire layer obtained by integration of the full equations. In all cases $k_x = k_y = 4$, $q = \frac{3}{2}\pi$, and $R = 4$; in (e) – (h), $\Lambda = 10^6$. The velocity perturbation, v_z, is shown in (a) and (e); the vorticity perturbation, ω_z, in (b) and (f); the magnetic field perturbation, $-ib_z$, in (c) and (g); the electric current perturbation, $-ij_z$, in (d) and (h).

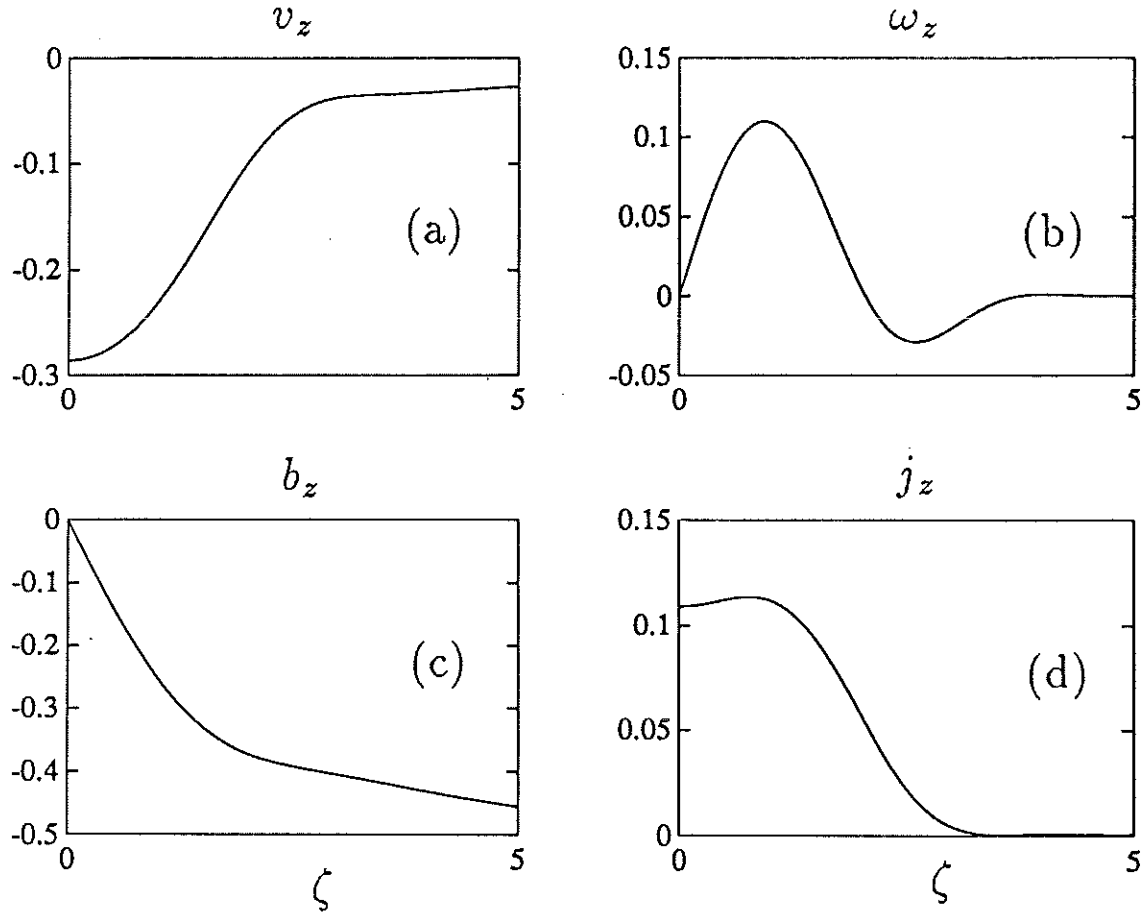
v_z
0
-0.1
-0.2
-0.3
0
5
(a)
ω_z
0.15
0.1
0.05
0
-0.05
0
5
(b)
b_z
0
-0.1
-0.2
-0.3
-0.4
-0.5
0
5
(c)
ζ
j_z
0.15
0.1
0.05
0
0
5
(d)
ζ

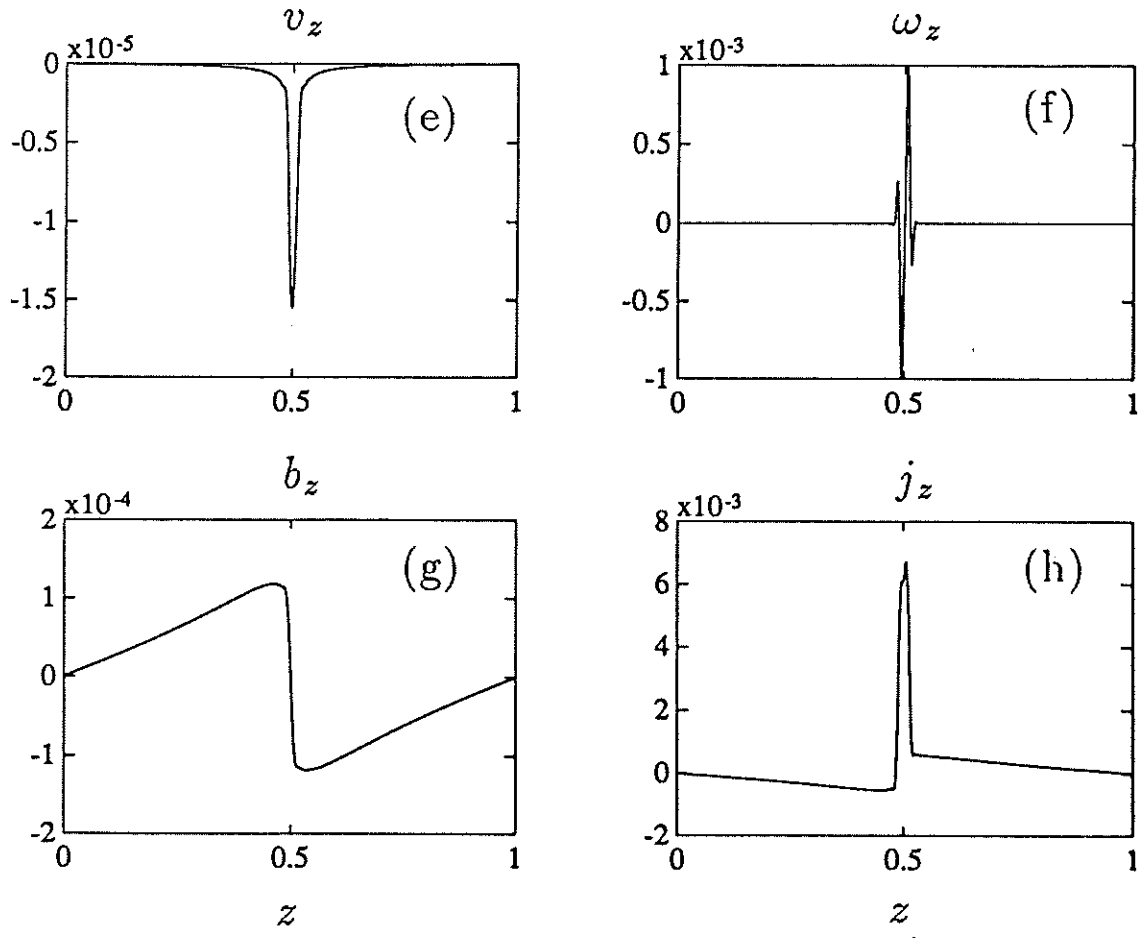
v_z
x10-5
0
-0.5
-1
-1.5
-2
0
0.5
1
(e)
ω_z
x10-3
1
0.5
0
-0.5
-1
0
0.5
1
(f)
b_z
x10-4
2
1
0
-1
-2
0
0.5
1
(g)
z
j_z
x10-3
8
6
4
2
0
-2
0
0.5
1
(h)
z

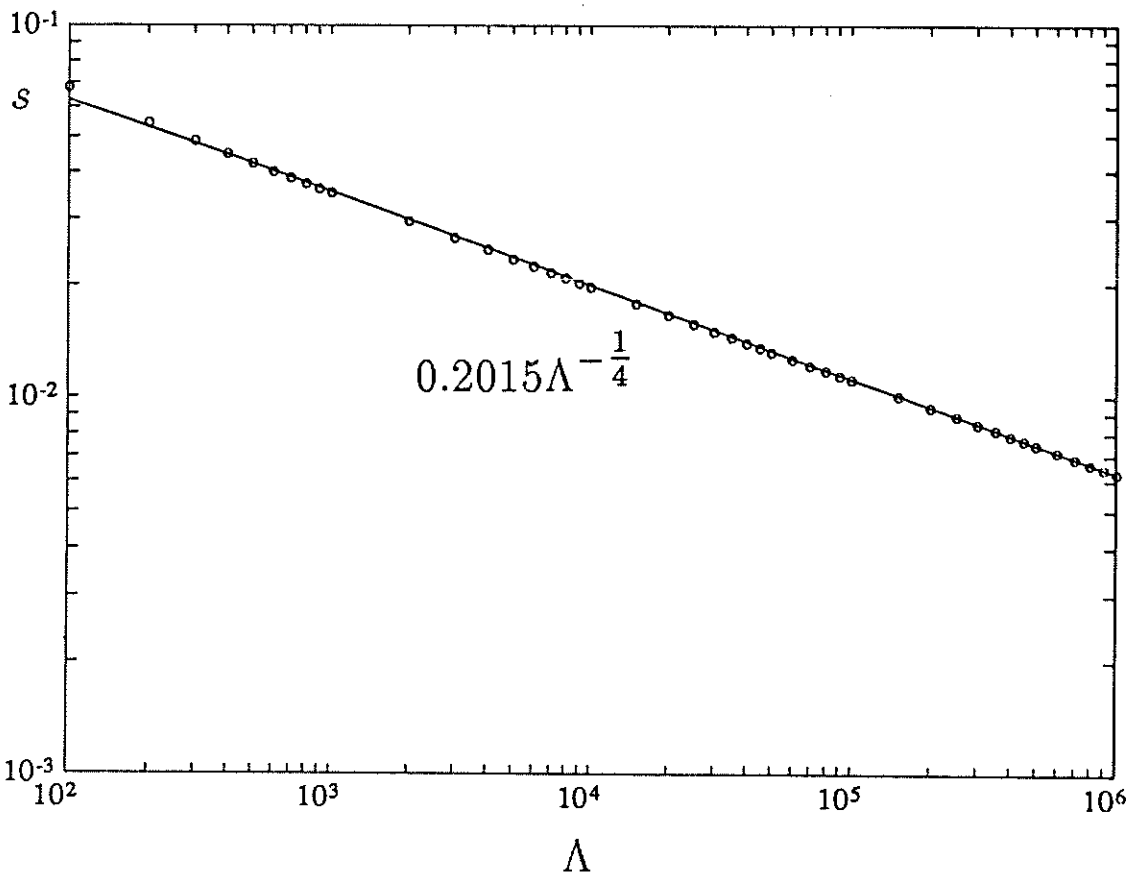

Figure 8(a). Log-log plot of the growth rate, s, of resistive instabilities as a functions of Λ for fast g-modes when there is one critical level in the layer: $q = \frac{3}{2}\pi$ and $R = 0.5(< R_c)$. In the case shown, $k_x = k_y = \Lambda^{1/4}$.

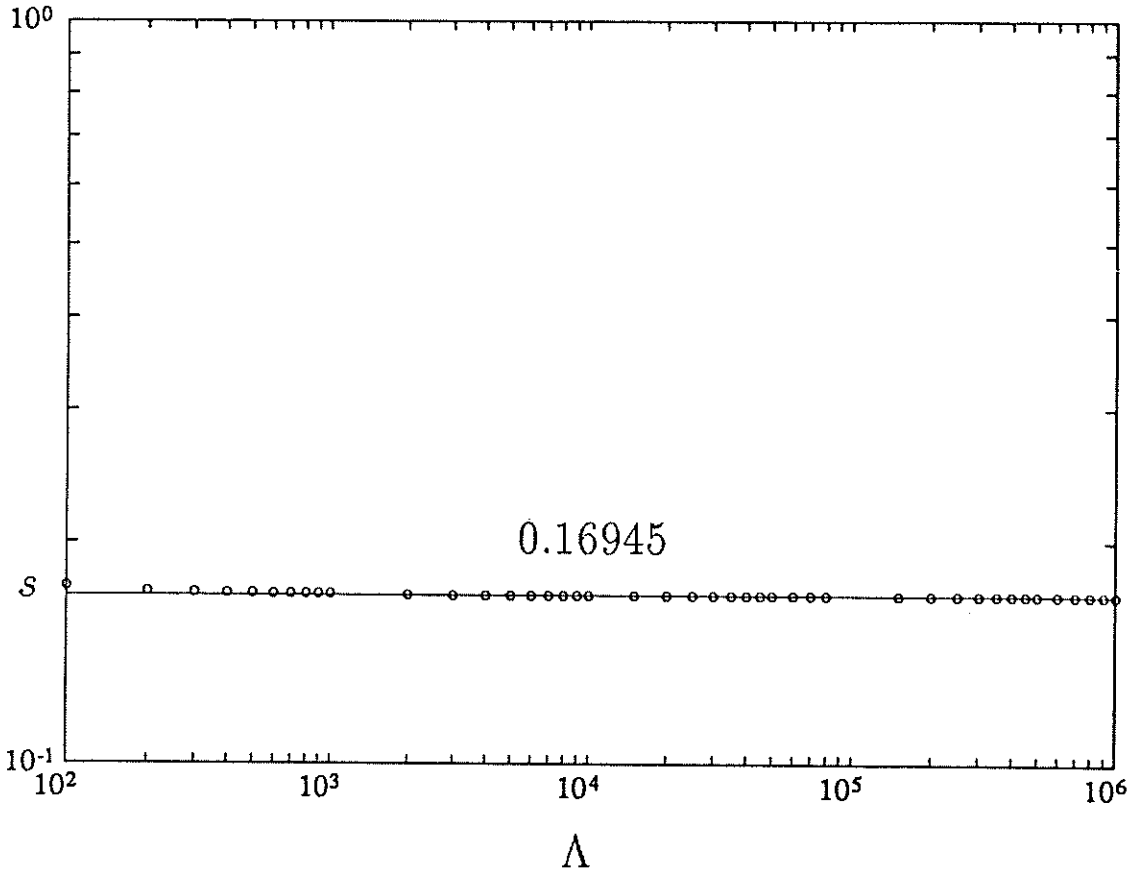

Figure 8(b). Log-log plot of the growth rate, s, of resistive instabilities as a functions of Λ for fast g-modes when there is one critical level in the layer: $q = \frac{3}{2}\pi$ and $R = 0.5(< R_c)$. In the (critical) case shown, $k_x = k_y = \Lambda^{1/2}$.

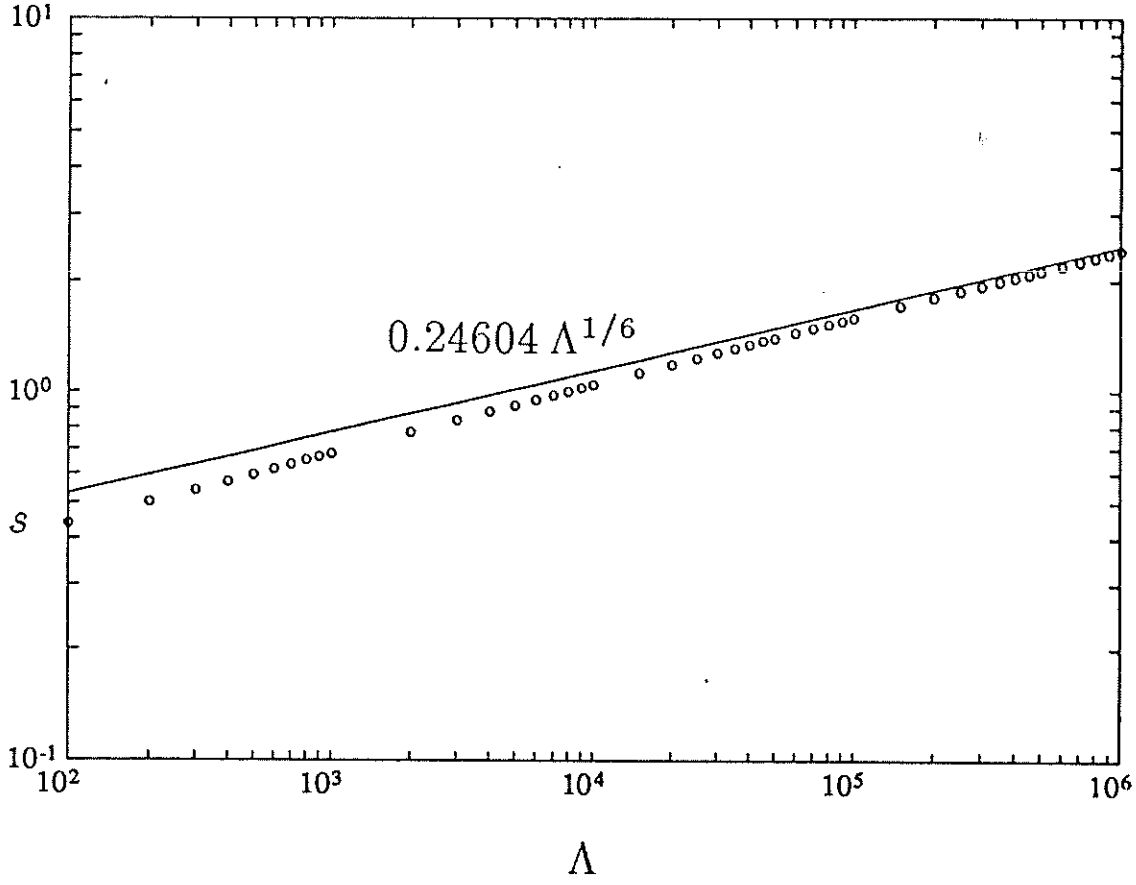

Figure 8(c). Log-log plot of the growth rate, s, of resistive instabilities as a functions of Λ for fast g-modes when there is one critical level in the layer: $q = \frac{3}{2}\pi$ and $R = 0.5(< R_c)$. In the case shown, $k_x = k_y = \Lambda^{3/4}$.

For Figures 9 see following page.

Figures 9. Comparisons between the eigenfunctions [(a) – (d)] for the fast g-mode in the critical layer in the limit $\Lambda \rightarrow \infty$ with the eigenfunctions [(e) – (h)] in the entire layer obtained by integration of the full equations. In all cases $k_x = k_y = \Lambda^{1/2}$ (a critical case), $q = \frac{3}{2}\pi$, and $R = 0.5$; in (e) – (h), $\Lambda = 10^5$. The velocity perturbation, v_z, is shown in (a) and (e); the vorticity perturbation, ω_z, in (b) and (f); the magnetic field perturbation, $-ib_z$, in (c) and (g); the electric current perturbation, $-ij_z$, in (d) and (h).

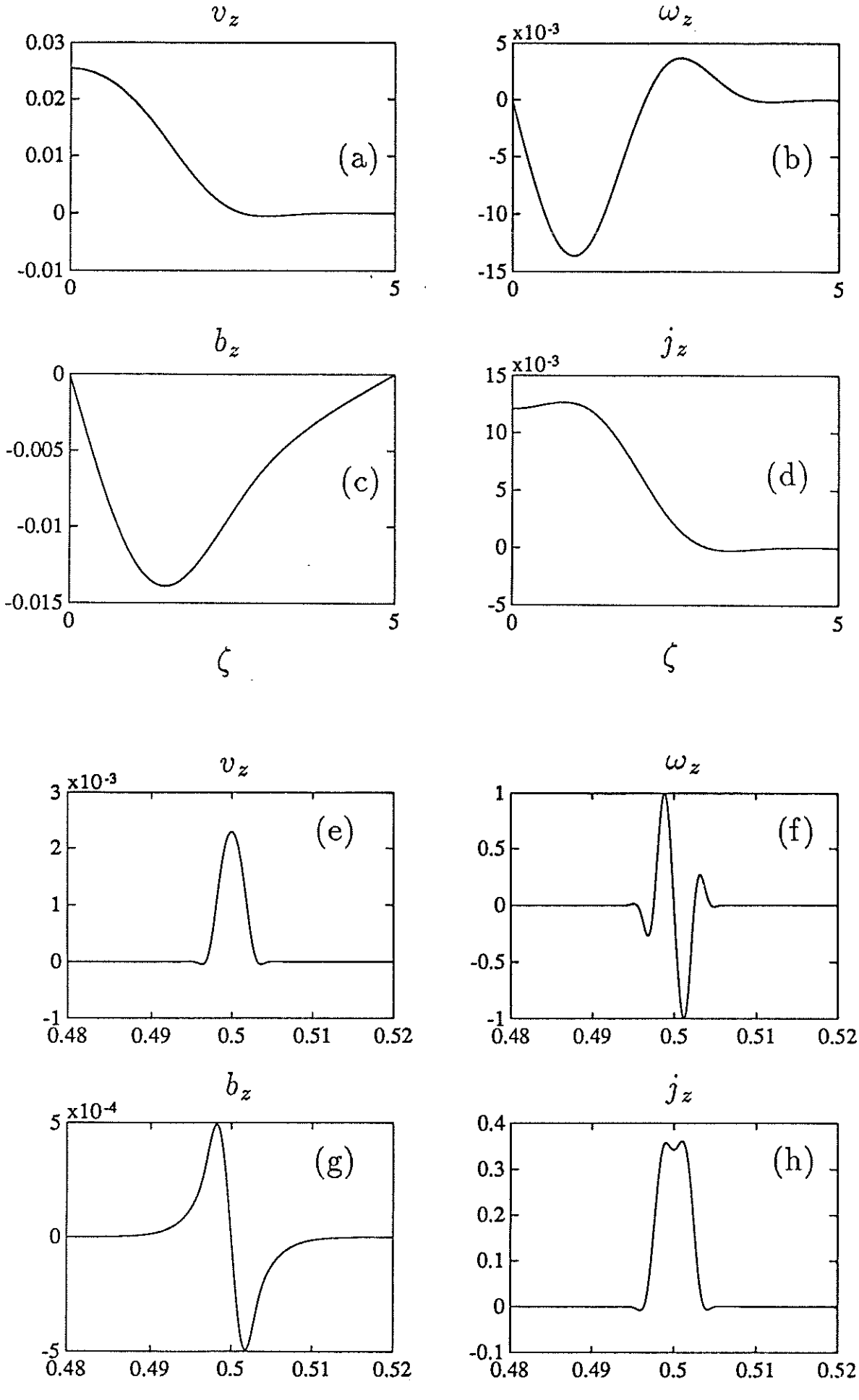
v_z
0.03
0.02
0.01
0
-0.01
0
5
(a)
ω_z
x10-3
5
0
-5
-10
-15
0
5
(b)
b_z
0
-0.005
-0.01
-0.015
0
5
(c)
j_z
x10-3
15
10
5
0
-5
0
5
(d)
ζ
ζ
v_z
x10-3
3
2
1
0
-1
0.48
0.49
0.5
0.51
0.52
(e)
ω_z
1
0.5
0
-0.5
-1
0.48
0.49
0.5
0.51
0.52
(f)
b_z
x10-4
5
0
-5
0.48
0.49
0.5
0.51
0.52
(g)
j_z
0.4
0.3
0.2
0.1
0
-0.1
0.48
0.49
0.5
0.51
0.52
(h)
z
z